THE PRE-MAIN SEQUENCE EVOLUTIONARY MODELS OF LOW MASS STARS IN THE MASS RANGE 0.30 $M_\odot$– 0.60 $M_\odot$

A Ph.D. Thesis

Presented by

İbrahim KÜÇÜK

to

the Graduate School of Natural and Applied Sciences

of Middle East Technical University

in Partial Fulfillment for the Degree of

DOCTOR OF PHILOSOPHY

in

PHYSICS

MIDDLE EAST TECHNICAL UNIVERSITY

ANKARA

April 1993

Approval of the Graduate School of Natural and Applied Sciences.

Prof. Dr. O. Alpay ANKARA
Director

I certify that this thesis satisfies all the requirements as a thesis for the degree of Doctor of Philosophy.

Prof. Dr. Şinasi ELLİALTIOĞLU
Chairman of the Department

We certify that we have read this thesis and that in our opinion it is fully adequate, in scope and quality, as a thesis for the degree of Doctor of Philosophy in Physics.

Prof. Dr. Dilhan ERYURT-EZER
Supervisor

Examining Committee in Charge:

Prof. Dr. Cemal AYDIN(Chairman)
Prof. Dr. Dilhan ERYURT-EZER
Prof. Dr. Halil KIRBIYIK
Prof. Dr. Ümit KIZILOĞLU
Assoc. Prof. Dr. Nilgün KIZILOĞLU

ABSTRACT

THE PRE-MAIN SEQUENCE EVOLUTIONARY MODELS OF LOW MASS STARS IN THE MASS RANGE 0.30 $M_\odot$– 0.60 $M_\odot$

KÜÇÜK, İbrahim

Ph. D. in Physics

Supervisor: Prof. Dr. Dilhan ERYURT-EZER

April 1993, 60 pages.

In this thesis, stellar evolutionary models of stars of low mass in the mass range of 0.30 through 0.60$M_\odot$ are presented. For that purpose Eryurt–Ezer[25]'s stellar evolutionary program is used and modified for low mass stars of our interest. An initial chemical composition of X=0.739, Y=0.240, Z=0.021 for mixing–length, l/H_p ratio of 1.3 were chosen. Each model has started from threshold of stability and the evolution has followed through the zero age main sequence (ZAMS) up to a point at which the hydrogen content has been reduced to about 0.600.

The physical input has been improved with the adoptation of the recent values of thermonuclear reaction rates (Fowler et al.[18] and Harris et. al.[19]). Since in these high density low mass stars the electron screening plays an important role in calculating the thermonuclear reaction rates, particular attention has been given to the treatment of the electron screening factors. For this purpose we have used screening factors calculated by the method given by Itoh et. al.[21]. The effect of pressure ionization has been treated by the method of Rouse[20].

The $0.30M_{\odot}$ star develops a small radiative core but reaches the ZAMS as a wholly convective star. As going from $0.30M_{\odot}$ to $0.60M_{\odot}$ the time the stars spend during gravitational contraction phase gets shorter. The size of the convective cores, which develops when the energy generated by nuclear burning becomes comparable with gravitational contraction energy, gets smaller while going from $0.40M_{\odot}$ to $0.60M_{\odot}$.

The zero age evolutionary times for 0.30, 0.40, 0.50 and $0.60M_{\odot}$ stars are found to be 6.95×10^{8}, 3.57×10^{8}, 3.46×10^{8} and 1.89×10^{8} years, respectively.

A comparison of results of the present study with recent observational results of low mass stars of our interest and T Tauri stars are presented. This led us to the conclusion that HR 6426 B is a star near ZAMS. The estimated evolutionary time is about $t=1.08\times10^{8}$ yr. with central temperature and density of 9×10^{6} K^{0} and 78 gr/cc, respectively.

An upper limit to the ages for T Tauri stars, $\sim 6\times10^{6}$yr., which is found from isochrones drawn from theoretical results seems to be in agreement with the estimates of $\sim 5\times10^{6}$yr. by Herbig[33].

Keywords : Stellar Evolution, Low Mass Stars, Pre–Main Sequence Evolutionary Tracks, Convective Stars, T Tauri Stars, Reaction Rates, Electron Screening.

Science Code : 402.02.01

ÖZ

0.30 $M_\odot$– 0.60 $M_\odot$ ARASI KÜÇÜK KÜTLELİ YILDIZLARIN ANA KOL ÖNCESİ EVRİM MODELLERİ

KÜÇÜK, İbrahim

Doktora Tezi, Fizik Anabilim Dalı

Tez Yöneticisi: Prof. Dr. Dilhan ERYURT-EZER

Nisan 1993, 60 sayfa.

Bu tezde kütleleri $0.30 - 0.60 M_\odot$ arasında olan küçük kütleli yıldızların evrim modelleri verilmektedir.

Bu amaçla Eryurt–Ezer[25] yıldız evrim programı küçük kütleli yıldızlar için gerekli ilaveler yapılarak kullanılmıştır. Başlangıç kompozisyonu olarak X=0.739, Y=0.240, Z=0.021, karışma uzunluğu için ise l/H_p=1.3 değerleri kullanılmıştır. Her model kararlılık aşamasından başlatılmış, evrim yolu yıldız sıfır yaş ana–kol konumuna eriştikten sonra hidrojen miktarı $\sim$ 0.600 değerine düşene kadar sürdürülmüştür.

Fiziksel girdiler en yeni reaksiyon oranları (Fowler et al.[18] and Harris et. al.[19]) kullanılarak geliştirilmiş ve yüksek yoğunluğa sahip olan küçük kütleli yıldızlarda elektronların perdeleme etkilerinin reaksiyon oranlarının hesabında önemli rol oynaması nedeniyle perdeleme etkisi faktörleri hesabına ayrı bir önem verilmiştir. Bu amaçla Itoh et. al.[21] tarafından verilen yöntem ile hesaplanan perdeleme etkisi faktörleri kullanılmıştır. İyonlaşma basıncı etkisi için Rouse[20] yöntemi dikkate alınmıştır.

$0.30M_{\odot}$ kütleli yıldız küçük bir radyatif çekirdek oluşturmasına rağmen sıfır yaş ana kol'una tamamen konvektif bir yapıya sahip olarak ulaşmaktadır. $0.30M_{\odot}$ kütleli yıldızdan $0.60M_{\odot}$ kütleli yıldıza gidildikçe yıldızların çekimsel büzülme evresinde harcadıkları zaman kısalmaktadır.

Nükleer reaksiyonlardan dolayı açığa çıkan enerjinin çekimsel büzülme enerjisi ile aynı olmaya başladığı zaman oluşan konvektif çekirdek büyüklüğünün $0.40M_{\odot}$ kütleli yıldızdan $0.60M_{\odot}$ kütleli yıldıza gidildikçe azalmakta olduğu görülmüştür.

0.30, 0.40, 0.50 and $0.60M_{\odot}$ kütleli yıldızların sıfır yaş ana kol'una erişme zamanları ise sırasıyla 6.95×10^{8}, 3.57×10^{8}, 3.46×10^{8} ve 1.89×10^{8} yıl olarak bulunmuştur.

Elde edilen sonuçların ilgili küçük kütleli yıldızların en yeni gözlemsel sonuçları ve T Tauri yıldızları ile karşılaştırması verilmiştir. Buradan HR 6426 B yıldızının sıfır yaş ana kol'u yakınlarında bir yıldız olduğu sonucuna varılmıştır. Belirlenen evrim zamanı 1.08×10^{8} yıl, merkezi sıcaklık ve yoğunluk ise, sırasıyla, 9×10^{6} K^{0} ve 78 gr/cc 'dir.

T Tauri yıldızlarının yaş tayini için kuramsal sonuçlardan elde edilerek çizilen eşit yaş çizgilerinden bulunan $\sim6\times10^{6}$yıllık üst limit Herbig[33] tarafından verilen $\sim 5\times10^{6}$yıl değeri ile uyum göstermektedir.

Anahtar kelimeler :Yıldızların Evrimi, Küçük Kütleli Yıldızlar, Ana–Kol Öncesi Evrim Yolları, Konvektif Yıldızlar, T Tauri Yıldızları, Reaksiyon Oranları, Elektronların Perdeleme Etkileri.

Bilim dalı sayısal kodu : 402.02.01

ACKNOWLEDGEMENTS

I am deeply thankful to my supervisor Prof.Dr. Dilhan Eryurt-Ezer for her valuable guidance and her continued encouragements and suggestions throughout this work.

I am very grateful to Assoc. Prof. Dr. Nilgün Kızıloğlu for her encouragements and helps to understand the "Stellar Evolutionary Program" at any time I need, and to Prof. Dr. Cemal Aydın, Prof. Dr. Halil Kırbıyık, and to Prof. Dr. Ümit Kızıloğlu for reading the manuscript.

I would like to thank to Res. Asst. Bülent Uyanıker for his comments and especially for his helps during editing the text and plotting the figures using new version of "Grapher".

I also would like to thank to Prof. Dr. Ay Melek Özer for allowing to use their group computer at any time I need.

Special thanks are to my all friends in Physics Department.

Finally, I would like to thank my family for their moral supports and encouragements.

TABLE OF CONTENTS

Page

LIST OF TABLES

LIST OF FIGURES

CHAPTER I

INTRODUCTION

The behaviour of stellar objects near the bottom of the main sequence is a topic of great interest for studies of stellar populations and galactic structure. Investigating the lower end of the main sequence is interesting since it is currently believed that an appreciable fraction of the mass in most galaxies resides in the form of low mass stars. Although the intrinsic faintness of these objects makes them difficult to study, significant observational progress has been made during past decade. Because of their long evolutionary time scales, they are believed to burn hydrogen in their centers. The high densities and low temperatures of these stars bring some problems for the calculation of the structure of their interiors.

Models of stars on the Lower Main Sequence (LMS) have been constructed by numerous investigators with much of the pioneering work being carried out by Hayashi and Nakano[1], and Ezer and Cameron[2]. These studies demonstrated that the size of the radiative cores decreases with decreasing mass and that at $\sim 0.30M_{\odot}$, the stellar interiors become completely convective. Moreover, it was shown that stars with mass of $\leq 0.10M_{\odot}$ could not achieve a state of thermal equilibrium by burning hydrogen.

More recent investigations of the LMS have been carried out by Copeland et.al. [3] (hereafter CJJ); Hoxie [4]; Grossman et. al.[5](hereafter GHG);
Sienkiewicz [6]; VandenBerg et. al.[7](hereafter VHDA); Rappaport and Joss [8]; Neece [9]; D'Antona and Mazzitelli [10](hereafter DM); Nelson et. al.[11](hereafter NRJ); and Dorman et. al.[12](hereafter DNC).

One of the most comprehensive early studies of the evolutionary sequences of models of stars of low mass was carried out by Ezer and Cameron [2]. They found that the $0.30M_{\odot}$ star develops a radiative core before reaching the main sequence, but the $0.20M_{\odot}$ star reaches the main sequence as a wholly convective star. They also showed that the limiting mass for the stars to become completely degenerate is $0.10M_{\odot}$.

CJJ[3] systematically investigated the structure of chemically homogeneous Population I and II stars assuming various compositions and different values for the mixing lengths, l.

GHG[5] have investigated the structure of stars on the theoretical low mass main sequence for the mass range $0.085 - 0.50M_{\odot}$. They have chosen a chemical composition of X=0.68, Z=0.03 and l/H_p ratio of 1.

Sienkiewicz [5] has presented a comparison between observational and theoretical parameters of the very low mass ($M < 0.30M_{\odot}$) hydrogen (X=0.7) main sequence stars

The VHDA[7] models presented in Table −4.5 are ZAMS models taken from evolutionary calculation initiated on the Hayashi track (X=0.7, Z=0.02; l/H_p=1). They used Eggleton, Faulkner, and Flannery [13](hereafter EFF) equation of state (EOS) and Alexander opacities.

Neece[9] computed static stellar models in the mass range of $0.15 - 0.55M_{\odot}$ for a chemical composition of X=0.68, Z=0.03, and l/H_p=1. He used the Cox−Tabor[14] opacities augmented by Los Alamos tables.

DM[10] investigated the structure and evolution (including pre−main sequence evolution) of LMS stars and brown dwarfs in the mass range of $0.04 - 0.60M_{\odot}$. They employed the EOS of Magni and Mazzitelli[15] for the chemical composition of X=0.73 and Z=0.02 together with Alexander, Johnson, and Rypma[16] opacities.

The results of NRJ[11] are based on modified n=3/2 polytropes representing stars for a chemical composition of X=0.7 and Z=0.02. The opacities

used are those of Alexander[17] and Coulombic interactions are incorparated in the EOS for the interior.

DNC[12] have calculated theoretical models of stars on the hydrogen−burning LMS having masses $<0.55M_{\odot}$. Particular attention has been done in the treatment of the atmosphere and envelope and to the choice of the radiative opacities and EOS.

Theoretical calculations of stars on the LMS have differed in several important ways. For example, various numerical approaches have been used to construct the models. Moreover, the formulation and implementation of the input physics have varied greatly. The properties of these stellar models over a mass range of our interest with different compositions are listed in Table−4.5.

The first aim of the present study is the construction of the evolutionary sequence of theoretical models of low mass stars in the mass range $0.30 - 0.60M_{\odot}$, by using solar abundance values of X=0.739, Y=0.240, Z=0.021, starting from threshold of stability (which will be described in Chapter II) through gravitational contraction phase, up to the zero age main−sequence, secondly to compare our stellar models with observed low mass stars of our interest.

The physical input in the present study has been improved in the following features over the ones that at previous study.

The recent values of thermonuclear reaction rates given by Fowler et al.[18] and Harris et. al.[19] has been used. Since the pressure ionization plays an important role in low mass stars, we employed the method of Rouse[20] to treat pressure ionization. Because in these high density and relatively low temperature low mass stars, electron screening becomes important in calculating the thermonuclear reaction rates, particular attention has also been paid to the treatment of electron screening factors. We have used new electron screening factors of Itoh et. al.(hereafter IHS)[21] which are appropriate to the temperatures and densities found in present models.

CHAPTER II

CONSTRUCTION OF STELLAR MODELS

The evolution of a star can be described by the functions

$$T(M_r, t),\ r(M_r, t),\ \varrho(M_r, t),\ L_r(M_r, t),\ X_i(M_r, t)$$

where M_r is the mass of a sphere of radius r, ϱ is the density, T is the temperature, L_r is the net outward flow of energy accross a sphere of radius r, X_i is the mass fraction of element i and t is the time. At any particular time, t, the run of the physical variables from M_r=0 to M_r=M_{tot} constitutes a stellar model. An evolutionary track is a sequence of stellar models calculated for a closely spaced and monotonically increasing set of time values. If the time variation of the physical parameters is taken to be small, the stellar models in an evolutionary track can be represented by models which are in equilibrium.

2.1 Basic Structure Equations

Assuming that the star is a spherically symmetric, self gravitating perfect fluid(all the physical variables depend only on the mass M and the rotation and magnetic effects are not included). Then the time−independent equilibrium structure equations governing the internal structure are the following:

$$\frac{dr}{dM} = \frac{1}{4\pi r^2 \varrho} \tag{2.1}$$

$$\frac{dP}{dM_r} = -\frac{GM_r}{4\pi r^4} \tag{2.2}$$

$$\frac{dL}{dM_r} = \epsilon_{tot} = \epsilon_{nuc} + \epsilon_G - \epsilon_\nu \tag{2.3}$$

The energy transport equation is written as

$$\frac{dT}{dM_r} = -\frac{G}{4\pi r^4}\frac{M_r T}{P}\nabla_c \qquad \text{convective transport} \tag{2.4}$$

$$\frac{dT}{dM_r} = -\frac{G}{4\pi r^4}\frac{M_r T}{P}\nabla_{rad} \qquad \text{radiative transport} \tag{2.5}$$

where

$$\nabla_c = (\frac{dlnT}{dlnP})_c \tag{2.6}$$

and

$$\nabla_{rad} = (\frac{dlnT}{dlnP})_{rad} = \frac{3\chi P L_r}{64\pi\sigma T^4 G M_r} \tag{2.7}$$

In the above equations M_r is the mass inside a sphere of radius r, ϱ the density, ϵ the energy generated per gram per sec., L_r energy traversing the sphere of radius r per sec., χ is the mean mass absorption coefficient (or opacity), σ is the Stephan–Boltzmann constant, G is the gravitational constant, P the total pressure and T is the temperature.

ϵ_ν and ϵ_{nuc} are the energy removed by neutrinos and the energy generated by nuclear reactions per unit mass per unit time, respectively. ϵ_G is the gravitational energy released as a result of contraction of the star per unit mass per unit time and will be explained in next chapter.

Equations (2.1) and (2.2) express the the spherical distribution of the mass and the hydrostatic equilibrium condition, respectively.

They result from the stability condition that the gravitational force acting on any point of the star must be balanced by the pressure at the same point.

Equation (2.3) is the law of conservation of energy in differential form. The total energy loss per unit time, crossing the sphere of radius r, is characterized by the luminosity L_r. The last two equations (2.4) and (2.5) express the transport of energy produced. The two cases of transport mechanism are either convective or radiative transfer.

The constitutive relations supplying the differential equations governing the structure of the star and describing the physical properties of the gas are:

$$P = P(\varrho, T, \mu) \qquad \text{Equation of State} \tag{2.8}$$
$$\chi = \chi(\varrho, T, \mu) \qquad \text{Opacity}$$
$$\epsilon_{nuc} = \epsilon_{nuc}(\varrho, T, \mu) \qquad \text{energy generation}$$

For the differential equations (2.1) through (2.5) the following boundary conditions are applied:

−At the center, where the total mass M=0, the luminosity L and radius R are both equal to zero, i.e,

$$L = R = 0 \tag{2.9}$$

−At the surface of the star, the photospheric pressure P_{ph} can be derived from

$$\frac{dP_{ph}}{d\tau} = \frac{GM}{R^2\chi} \tag{2.10}$$

assuming that τ=τ_{BD} and P=P_{ph} and χ=constant (or χ=$\chi_{surface}$) at the stellar surface. Eddington's approximation states that

$$T^4 = \frac{3}{4}T_{eff}^4(\tau + \frac{2}{3}) \tag{2.11}$$

We can conclude that at the optical depth τ=2/3 the surface temperature is

$$T = T_{eff} \tag{2.12}$$

which is obtained from the concept of the radiative transfer in stellar atmospheres of the stars and corresponds approximately to the temperature at this optical depth. The effective temperature T_{eff} and the photospheric pressure P_{ph} are written as

$$T_{eff}^4 = \frac{L}{4\pi R^2\sigma} \tag{2.13}$$

$$P_{ph} = \frac{GM\tau_{BD}}{R^2\chi} \tag{2.14}$$

where L is the average luminosity at the surface and R and M are the total radius and total mass of the star, respectively. τ_{BD} denotes the optical depth at the stellar surface. Where

$$F = \frac{L}{4\pi R^2} \tag{2.15}$$

is the radiation flux by definition.

2.2 Convection Theory

The pre−main sequence evolutionary tracks of low mass stars, which are characterized by models having deep convective regions are very sensitive to the treatment of the convection. Considering low mass stars having masses $M \leq 0.30\odot$, the structure becomes fully convective. So, it will be better to review the mixing−length theory of convection.

Equations (2.4) and (2.5) define the energy transport mechanisms. If the energy is tranported through the star by radiation, for instance, the temperature gradient $\frac{dT}{dM_r}$ contains the local values of opacity, radius and net outward rate of flow of energy through a sphere of radius r by equation (2.5). If radiative equilibrium becomes unstable and the energy is carried by convective motion of the gas then Equation (2.4) is used. The discussion whether the energy is transported by radiation or by convection is given by Schwarzchild criterion, that is, when the radiative temperature gradient, ∇_{rad}, becomes greater than the adiabatic temperature gradient, ∇_{ad}, i.e.

$$\nabla_{rad} > \nabla_{ad} \tag{2.16}$$

then, the energy is believed to be transported by convective motion of the gases. The basic problem for which the mixing−length theory is used can be summarized as follows:

Given the situation $\nabla_{rad} \geq \nabla_{ad}$ at some region inside a star, what about the

values of the convective flux, F_{con}, and the actual temperature gradient,

$$\nabla = (\frac{dlogT}{dlogP})_{actual}, \tag{2.17}$$

in the stellar gas at that region? In the present work the above stated quantities are obtained by using Prandtl's mixing–length theory in the form arranged by Böhm–Vitense [22].

The set of relevant quantities in the convective gas are:

1. l:distance the convective mass elements can move until they dissolve into the surrounding. In fact, it is the mean free path for the convective transport and known as mixing–length. In our stellar models it is in the form of $l=\alpha H_p$, where α is a constant, and H_p is the pressure scale height;

2. $\bar{v}$:average speed of the convective mass elements (It is assumed that convective mass elements at the same distance have the same speed);

3. t=$l/\bar{v}$: mean life time of a convective element (which is the average time that convective elements retain their identity);

4. T':average temperature of the convective elements;

5. T:average temperature of the surrounding;

6. z:position coordinate of the rising and falling convective elements;

7. $\frac{dT'}{dz}$:linear gradient for the average temperature of a moving convective element;

8. $\frac{dT}{dz}$:linear gradient for the average temperature of surrounding;

Inside the moving element, the total flux can be written as:

$$F_{total} = F_{rad} + F_{con} \tag{2.18}$$

where

$$F_{rad} = (\frac{4ac}{3})(\frac{T^3}{\chi\varrho})\frac{dT}{dr} \tag{2.19}$$

is the radiative flux due to Equation (2.5) and F_{con} is the convective flux which we want to define.

Let, z be the position coordinate of the convective element. The temperature excess of the moving element over its surrounding and over a distance z will be

$$\Delta\bar{T} = \int_0^z (\frac{dT'}{dz} - \frac{dT}{dz})dz \tag{2.20}$$

If we assume that $\frac{dT'}{dz}$and$\frac{dT}{dz}$ are constants over z, then

$$\Delta\bar{T} = (\frac{dT'}{dz} - \frac{dT}{dz})z. \tag{2.21}$$

The convective flux which is the heat transfer per unit time per unit area, is written as

$$F_{con} = \Delta\bar{T}\bar{v}\varrho c_p \tag{2.22}$$

where c_p is the average value (over a distance z) of specific heat at constant pressure.

Now, let us determine the average speed $\bar{v}$ of the convective elements. When the element moves upward there will be a density excess ϱ=ϱ(P,T,μ). One can determine the derivative of the density as

$$\partial\varrho = (\frac{\partial\varrho}{\partial P})_{T,\mu}dP + (\frac{\partial\varrho}{\partial T})_{P,\mu}dT + (\frac{\partial\varrho}{\partial\mu})_{P,T}d\mu \tag{2.23}$$

The first term on the right hand side of the above equation goes to zero due to the pressure equilibrium. Then, it becomes

$$\frac{\partial\varrho}{\varrho} = \frac{\partial T}{T}[\frac{T}{\varrho}(\frac{\partial\varrho}{\partial T})_{P,\mu} + \frac{T}{\varrho}(\frac{\partial\varrho}{\partial\mu})_{P,T}(\frac{\partial\mu}{\partial T})_P] \tag{2.24}$$

and rewriting we have

$$\frac{\partial\varrho}{\varrho} = \frac{\partial T}{T}[(\frac{\partial ln\varrho}{\partial lnT})_{P,\mu} + (\frac{\partial ln\varrho}{\partial ln\mu})_{P,T}(\frac{\partial ln\mu}{\partial lnT})_P]. \tag{2.25}$$

Defining

$$f(\varrho, T, P, \mu) = -[(\frac{\partial ln\varrho}{\partial lnT})_{P,\mu} + (\frac{\partial ln\varrho}{\partial ln\mu})_{P,T}(\frac{\partial ln\mu}{\partial lnT})_P]. \tag{2.26}$$

and using (2.25) and (2.26) we have the relation for the density defficiency

$$-\frac{\partial\varrho}{\varrho} = \frac{\partial T}{T}f(\varrho, T, P, \mu). \tag{2.27}$$

If we consider the moving convective element in the upward direction it gains kinetic energy

$$\frac{1}{2}mv^2 = \int_0^z K(z)dz \tag{2.28}$$

where K(z) is known as buoyant force which is the net force on the volume of the element and can be written as

$$K(z) = -g\Delta\varrho \times volume. \tag{2.29}$$

Using (2.27) and (2.29) we get

$$\frac{1}{2}mv^2 = \int_0^z g\varrho\frac{\partial T}{T}f(\varrho, T, P, \mu)dz \times volume. \tag{2.30}$$

Since volume is m/ϱ of the convective element and

$$\partial T = (\frac{dT'}{dz} - \frac{dT}{dz})z \tag{2.31}$$

Then

$$\frac{1}{2}v^2 = g\int_0^z (\frac{dT'}{dz} - \frac{dT}{dz})\frac{f(\varrho, T, P, \mu)}{T}zdz \tag{2.32}$$

here g is assumed to be constant along the distance z. Integrating (2.32)

$$\bar{v}^2 = g\frac{f(\varrho, T, P, \mu)}{T}(\frac{dT'}{dz} - \frac{dT}{dz})z^2 \tag{2.33}$$

which is true for the upward or downward motion of the convective element. Taking z=$l/2$, then the average velocity of the moving convective element can be found to be

$$\bar{v} = \frac{l}{2}\sqrt{\frac{gf(\varrho, T, P, \mu)}{T}}(\frac{dT'}{dz} - \frac{dT}{dz})^{\frac{1}{2}}. \tag{2.34}$$

Using (2.31) together with (2.33) in (2.22) we get

$$F_{con} = \frac{1}{2}c_p l\bar{v}\varrho(\frac{dT'}{dz} - \frac{dT}{dz}) \tag{2.35}$$

This is the energy per unit mass per unit time carried by mass motions of convective elements.

Up to here, one can conclude that if the convective elements move adiabatically the flux will be as Equation (2.35). But the moving convective

elements also lose energy by radiation. As they rise a distance l, energy will be carried in the form of an excess of internal energy comparing to the surrounding. Supposing that the convective elements are optically thick, then the energy lost by the turbulent element during its lifetime by the radiation is

$$\Delta E = -k\frac{\partial Q}{\partial z} \times area \times t \tag{2.36}$$

where ∂Q is the temperature difference between the center of the turbulent element and its surrounding, ∂z is the distance over which this temperature difference occurs, and

$$k = \frac{4ac}{3\chi\varrho} T^3 \tag{2.37}$$

is the radiative coefficient [c.f. Equation (2.19)].

This lose or gain of heat may be regarded as "horizontal". Since there are, on the average, as many hot elements as cool ones over a spherical shell, there can be no direct contribution to the net "vertical" heat transport however, they contribute indirectly to the net outward heat flux through their effect on the efficiency of convection.

The loss of convective heat flux due to non−adiabatic effect is

$$\Delta E = (F_{con} - F_{ad.con}) \times volume \tag{2.38}$$

Then the horizontal temperature gradient can be written as

$$\frac{\partial Q}{\partial z} = (\frac{dT'}{dz} - \frac{dT}{dz}) \tag{2.39}$$

Equating (2.36) and (2.37) we get

$$-k(\frac{dT'}{dz} - \frac{dT}{dz}) \times area\frac{1}{\bar{v}} = \frac{1}{2}c_p l\varrho[\frac{\mathrm{dT'}}{\mathrm{dz}} - (\frac{\mathrm{dT}}{\mathrm{dz}})_{\mathrm{ad}}] \times \mathrm{volume}. \tag{2.40}$$

Assuming that the ratio of the volume to the area is 1/6, and also to generalize above equation a factor of 8/3 should be introduced for thin and thick optical limit one writes

$$\frac{\frac{dT'}{dz} - \frac{dT}{dz}}{(\frac{dT}{dz})_{ad} - \frac{dT'}{dz}} = \frac{1}{24}\frac{c_p\varrho^2\chi l\bar{v}}{\sigma T^3}. \tag{2.41}$$

Inserting (2.34) in (2.35) we have

$$F_{con} = \frac{l^2}{4} c_p \varrho \sqrt{\frac{gf(\varrho, T, P, \mu)}{T}} (\frac{dT'}{dz} - \frac{dT}{dz})^{\frac{3}{2}}. \tag{2.42}$$

For the adiabatic convection

$$F_{ad.con} = \frac{l^2}{4} c_p \varrho \sqrt{\frac{gf(\varrho, T, P, \mu)}{T}} [(\frac{dT}{dz})_{ad} - \frac{dT}{dz}]^{\frac{3}{2}}. \tag{2.43}$$

The Equations (2.22), (2.34), (2.41) can be arranged as

$$F_{con} = c_p \varrho T \frac{l}{2H_p} \bar{v}(\nabla - \nabla') \tag{2.44}$$

$$\bar{v} = \frac{l}{2} \sqrt{\frac{gf(\varrho, T, P, \mu)}{H_p}} (\nabla - \nabla')^{\frac{1}{2}} \tag{2.45}$$

$$\frac{\nabla - \nabla'}{\nabla' - \nabla_{ad}} = c_p \varrho T \frac{\chi \varrho l}{24 \sigma T^4} \bar{v} \tag{2.46}$$

$$F_{rad} = \frac{16 \sigma T^4}{3 \chi \varrho H_p} \nabla \tag{2.47}$$

Here ∇ represents the average temperature gradient of all the matter at a given distance, ∇' is the temperature gradient of a rising or falling element. And H_p is the pressure scale height defined as the distance that the pressure is changing inside the star by a factor of e (H_p=$P_g/g\varrho$). Then, the total flux is:

$$F_{rad} + F_{con} = F = \frac{L}{4\pi r^2} \tag{2.48}$$

Detailed discussion for the above formulation can be found elsewhere (Cox and Guili [23] and Motz[24]). Using the expressions given by the equations (2.45) through (2.48) the actual temperature gradient, ∇, can be obtained.

2.3 Method of Computation

The numerical integrations of the differential equations, Equations (2.1) through (2.5), with boundary conditions, Equations (2.8), were carried out by the Henyey Method which has been applied from the center all the way to the surface. The basic procedure to solve the system of differential equations at the center, at the surface, and at any intermediate region inside the star is explained elsewhere, Eryurt−Ezer[25].

This method involves dividing the interior region into mass shells of thickness ΔM_i. The differential equations of stellar structure are approximated by difference equations which use the values of the variables at the shell boundaries.

The starting of an evolutionary sequence requires an initial model. It was assumed that stars contract to the point of threshold of stability homologuously. Then, the zero time model corresponding to the point of threshold of stability can be obtained from the following considerations:
If the stars contract homologuously to that point, the energy balance equation can be written as

$$\frac{dL_r}{dM_r} = -\frac{\partial E}{\partial t} - P\frac{\partial}{\partial t}(\frac{1}{\varrho}) \tag{2.49}$$

The total energy E_T of the star in the present case is

$$E_T = E_{int} + E_G \tag{2.50}$$

where E_{int} is the internal energy, E_G is the gravitational potential energy. Using the Virial Theorem one can get the relation between internal and gravitational potential energies as

$$E_{int} = -\frac{1}{3(\gamma-1)}E_G \tag{2.51}$$

where $\gamma=\frac{c_p}{c_v}$ is the ratio of the specific heats. This equation says that in equilibrium the total internal energy of a gaseous sphere is the fraction $\frac{1}{3(\gamma-1)}$ of the gravitational potential energy. Now,

$$E_T = -\frac{(3\gamma-4)}{3(\gamma-1)}E_G \tag{2.52}$$

with

$$E_G = -(\frac{3}{5-n})\frac{GM^2}{R} \tag{2.53}$$

or denoting q=$\frac{3}{5-n}$, where n is polytropic index, one can rewrite (2.53) as

$$E_G = -q\frac{GM^2}{R}. \tag{2.54}$$

Then,

$$E_T = -\frac{(3\gamma-4)}{(\gamma-1)(5-n)}\frac{GM^2}{R} \tag{2.55}$$

This is, in fact, nothing but the energy of the star with no nuclear energy sources. If one consider that the gas is monatomic and composed of radiation ($\gamma > 4/3$) Then, if the star is dispersed to infinity (at the beginning of formation of the star, R$\rightarrow \infty$) we see that E_T=0. When the star is condensed to a definite radius R then we have $E_T < 0$. This means that there is loss of energy and this is seen as radiation. So, the total energy of the star has decreased in shrinking from ∞ to the radius R. Then, the total energy must be decreased at a rate

$$-\frac{dE_T}{dt} = L(R). \tag{2.56}$$

Assuming q and M don't change, we reach

$$-\frac{dR}{dt} = \frac{R^2L(R)}{GM^2}\frac{(\gamma-1)(5-n)}{(3\gamma-4)}. \tag{2.57}$$

Defining

$$J = \frac{(\gamma-1)(5-n)}{(3\gamma-4)}. \tag{2.58}$$

we have

$$-\frac{1}{R}\frac{dR}{dt} = J\frac{L(R)R}{GM^2}. \tag{2.59}$$

It may be seen that we are expressing the reciprocal time for the contraction rate as a function of the ratio of the luminosity to a measure of the gravitational potential energy. The quantity J may be called the contracting parameter; it is one of the fundamental parameters that had to be adjusted. Now, stability

criterion is checked by computing the gravitational energy and the internal energy for the model. The radius of the initial model can be adjusted in such a way that the difference between the total gravitational energy and the internal energy is smaller than some value. This starting point is called as "Threshold of Stability" and known that it is a point at which the gravitational energy of the contracting protostar becomes just greater than the sum of thermal, dissociation and ionization energies of the gas. The value of J can be used to fix the radius of the initial model.

CHAPTER III

INPUT PHYSICS AND FORMULATION

In this chapter the fundamental relations determining the physical state of the stellar matter are discussed.

These relations include the equation of state, thermonuclear reaction rates and opacity of the stellar material.

In the construction of stellar models X=0.739, Y=0.240, and Z=0.021 values, for hydrogen, helium, and heavy elements respectively which are proper values for Population I type stars, are used as initial chemical composition.

3.1 Equation of State

In the present study, the pressure due to the non−degenerate ions, non-relativistic partially degenerate electrons and the radiation are taken into account in the equation of state.

The total pressure can be written as consisting three parts: the ion pressure P_i, the electron pressure P_e, and the radiation pressure

$$P = P_i + P_e + \frac{1}{3}aT^4 \tag{3.1}$$

where a is the radiation constant.

The pressure of the non-degenerate ion gas is given by

$$P_i = \frac{\Re}{\mu_i}\varrho T \tag{3.2}$$

where $\Re$ is the gas constant per mole. and μ_i is the mean molecular weight of the ion gas which, for ions of atomic weight A_i and mass abundance X_i can be

written as

$$\frac{1}{\mu_i} = \sum \frac{X_i}{A_i} \tag{3.3}$$

In the absence of electron degeneracy the electron pressure is given by

$$P_e = \frac{\Re}{\mu_e} \varrho T \tag{3.4}$$

where μ_e is the mean molecular weight per electron and is given by

$$\frac{1}{\mu_e} = \sum \frac{Z_i}{A_i} X_i \tag{3.5}$$

The gas pressure consists of the sum

$$P_g = P_i + P_e \tag{3.6}$$

The P_g and ϱ values will, in general, depend on the degree of ionization of the atomic species, degree of dissociation of molecular species, and the phase space density function of the free electrons at the particular N_e (concentration of electrons) and T. At relatively high densities, departures from the perfect gas law are obvious. In the case of partial electron degeneracy the ion and electron pressure are calculated using Fermi–Dirac functions. The cases for the free electrons are subdivided as follows:

a)Ideal electron gas (Maxwell–Boltzmann distribution)

b)Partially degenerate electron gas (Fermi–Dirac Statistics)

c)Completely degenerate electron gas (velocity distribution is determined by Fermi–Dirac Statistics).

Then, the electron pressure of the gas with a degeneracy parameter ψ is given, in general form, by

$$P_i = \frac{8\pi}{3h^3} \int_0^\infty \frac{p^3}{1 + exp(-\psi + \frac{E}{kT})} \frac{\partial E}{\partial p} dp$$

$$\frac{\varrho}{\mu_e} = \frac{8\pi m_p}{h^3} \int_0^\infty \frac{p^2}{1 + exp(-\psi + \frac{E}{kT})} dp, \tag{3.7}$$

where m_p is the mass of proton, h is the planck constant, k is the Boltzmann constant, and the kinetic energy E of an electron with momentum p and mass m

is

$$E = mc^2[(1 + (\frac{p^2}{m^2c^2}))^{\frac{1}{2}} - 1] \tag{3.8}$$

These expressions are valid for all densities and temperatures. They reduce to the perfect gas law for ψ <-4. For ψ >20 the gas becomes completely degenerate and in this case the electron pressure of non−relativistic gas is given by

$$P_e = \frac{h^2}{5m}(\frac{3}{8\pi})^{\frac{2}{3}}(\frac{\varrho}{\mu_e\mu_p})^{\frac{5}{3}}. \tag{3.9}$$

In the transition region, where the electron gas is partially degenerate but non−relativistic, the ion and electron pressure and density are represented by the following expressions:

$$\begin{aligned} P_i &= \frac{4\pi}{h^3}(2m_e)^{\frac{3}{2}}(kT)^{\frac{5}{2}}(\frac{\mu_e}{\mu_i})F_{\frac{1}{2}}(\psi), \\ P_e &= \frac{4\pi}{h^3}(2m_e)^{\frac{3}{2}}(kT)^{\frac{5}{2}}\frac{2}{3}F_{\frac{3}{2}}(\psi), \\ \varrho &= \frac{4\pi}{h^3}\mu_e m_p(2m_e kT)^{\frac{3}{2}}F_{\frac{1}{2}}(\psi), \end{aligned} \tag{3.10}$$

where

$$F_w(\psi) = \int_0^\infty \frac{u^w}{1 + exp(u - \psi)}du \tag{3.11}$$

is the Fermi−Dirac integral.

Including the above mentioned relations in our stellar evolution program Eryurt−Ezer[25], partial and complete non−relativistic degeneracy of the electrons are allowed in EOS.

The effect of pressure ionization in the Saha equation which has been proposed by Rouse[20] is adopted for the present study. In this method a probability function which can easily be applied to the standard low density form of the Saha equation is postulated. This function considers the behaviour of the ionization reaction as a whole rather than as made up of the detailed changes of ionization energies and partition functions of the participating species. The Saha equation can be rewritten in the following form

$$\frac{C_{p-1}}{C_p} = P_e K_p \phi_{p-1}(p) \tag{3.12}$$

where C_p is the concentration of the p^{th} ionization stage, $K_p(T)$ is a function of temperature

$$K_p(T) = \frac{h^3}{(2\pi m_e)^{\frac{3}{2}}}(kT)^{-\frac{5}{2}}\frac{B_{p-1}}{2B_p}exp[-(\frac{\chi_{k-1}}{kT})]$$

and ϕ_p represents a density dependent function that describes the probability that a p^{th} ion can exist at density ϱ in a mean atomic volume of radius r_0. Then

$$\phi_p = \phi(n, r_0) = exp[-(\frac{\gamma a_n}{r_0})^m] \tag{3.13}$$

where γ and m are constants to be determined, and a_n is the classical Bohr orbit for electrons in the quantum state with the principal quantum number n. ϱ and r_0 are related through

$$r_0 = [\frac{3Am_p}{4\pi\varrho}]^{\frac{1}{3}} \tag{3.14}$$

Here, m=3 and γ=1.5 values are proper values and adopted in the present study. One boundary condition on $\phi(r_0)$ must be such that Eq.(3.19) reduces to the standard Saha equation et infinite r_0.

$$\phi(r_0) \longrightarrow 1 \qquad as \qquad r_0 \longrightarrow \infty \tag{3.15}$$

Furthermore, as r_0 approaches zero, the ratio

$$\frac{C_{p-1}}{C_p}$$

must approach infinity as the ground state of p^{th} ionization stage will disappear.

$$\phi(r_0) \longrightarrow \infty \qquad as \qquad r_0 \longrightarrow 0 \tag{3.16}$$

3.2 Energy Generation

A posibble mechanical process generating the large amounts of energy radiated by a star is a slow contraction of the star, which releases the potential energy of the gravitational field. Although gravitational contraction cannot be the principal source of energy for a star, it may be important at certain stages in a star's development.

For stellar models in the gravitational contraction phase, the main source of energy is the gravitational energy, E_G. Toward the end of the gravitational contraction, with sufficient increase of the interior temperature, nuclear energy generation starts to contribute to the gravitational energy.

Energy generation from different branches of p−p chain and CNO bi−cycle reactions are displayed as follows:

PPI:

$H^1+H^1 \longrightarrow D^2+e^+ +\nu$

$D^2+H^1 \longrightarrow He^3+\gamma$

$He^3+He^3 \longrightarrow He^4+2H^1$

The first and second reactions have to take place twice for each one of the third reactions. Not all of the energy liberated contributes to the star's luminosity. Some of the energy liberated is carried away by the neutrinos and is lost.
This set of reactions is the main branch of proton−proton (p−p chain) reaction. Other branches are shown in below:

PPII:

$He^3+He^4 \longrightarrow Be^7+\gamma$

$Be^7 \longrightarrow Li^7+e^-$

$Li^7+H^1 \longrightarrow 2He^4$

PPIII:

$He^3 + He^4 \longrightarrow Be^7 + \gamma$

$Be^7 + H^1 \longrightarrow B^8 + \gamma$

$B^8 \longrightarrow B^8 + e^+ + \nu$

$Be^8 \longrightarrow 2He^4$

As a result of these three modes of p−p chain hydrogen is converted to helium.

Hydrogen burning can also take place in a somewhat different way, making use of the catalytic action of the carbon isotope, C^{12}. This set of reactions comprises the carbon cycle or a more elaborate scheme sometimes called the CNO bi−cycle, since carbon, nitrogen, and oxygen are all involved.

CNO bi−cycle:

$C^{12} + H^1 \longrightarrow N^{13} + \gamma$

$N^{13} \longrightarrow C^{13} + e^+ + \nu_e$

$C^{13} + H^1 \longrightarrow N^{14} + \gamma$

$N^{14} + H^1 \longrightarrow O^{15} + \gamma$

$O^{15} \longrightarrow N^{15} + e^+ + \nu_e$

$N^{15} + H^1 \longrightarrow C^{12} + He^4$

3.2.1 Thermonuclear Reaction Rates

To calculate the energy generated by nuclear reactions the reaction rate for the particular reaction should be known.

Let us first explain the terminology of reaction rates. A reaction in which a particle, a, interacts with a nucleus, X, to produce a nucleus, Y, and a new particle, b, is designated by

$$a + X \longrightarrow Y + b + Q \qquad or \qquad X(a,b)Y \tag{3.17}$$

where Q is the released energy in the reaction.

Considering a gas composed of two types of particles 1 and 2, the

number of reactions per gram per second can be written as

$$r = \frac{N_1 N_2 < \sigma v >}{(1 + \delta_{12})\varrho} \tag{3.18}$$

where ϱ is the total density of the gas, N_1 and N_2 are the numbers of atoms of 1 and 2, the Kronecker delta function, δ_{12}, is one if 1=2 and zero if 1≠2, $< \sigma v >$ is the reaction probability of two particles per unit volume per unit time.

For a gas of mass density, ϱ, the number density, N_i, of the nucleide, i, is often expressed in terms of its mass function, X_i, by the relation

$$N_i = \varrho N_A \frac{X_i}{A_i} \qquad \text{cm}^{-3} \tag{3.19}$$

where Avagadro's number N_A=6.022169×10^{23} $(\text{mole})^{-1}$, and A_i is the atomic mass of i in the atomic mass number. Assuming reaction of species 1 with species 2 then the probability of 1 to react with 2 will be

$$P_1 = N_2 < \sigma v > \tag{3.20}$$

The mean lifetime, $t_1(2)$, of nucleus 2 for interaction with nucleus 1 is given by the relation

$$\lambda_1(2) = \frac{1}{t_1(2)} = N_1 < \sigma v > = \varrho N_A \frac{X_1}{A_1} < \sigma v > \qquad \text{sec}^{-1} \tag{3.21}$$

where $\lambda_1(2)$ is the decay rate of 2 with 1.

Substituting the values of N_1, N_2 and $< \sigma$ v>, the unscreened reaction rate can be written as

$$r_{unscreened} = (\frac{AN_A}{A_1}) X_1 X_2 g \varrho exp(-\frac{B_6}{T_6^{\frac{2}{3}}}) T_6^{-\frac{2}{3}} \qquad (\text{gm - sec})^{-1} \tag{3.22}$$

where A is numerical constant.

$$A = 4.34 \times 10^5 \frac{(A_1 + A_2) S(0) B_6^2}{A_1^2 A_2 Z_1 Z_2} \tag{3.23}$$

with

$$B = \frac{3E_0}{k} T^{-\frac{2}{3}}$$

T_6 is the temperature in units of 10^6 K^0, E_0 is the energy in units of keV, S(0) is the astrophysical cross section factor at zero energy.

3.2.2 Screening Factors

In a dense gas, each nucleus attracts neighboring electrons and repels neighboring nuclei, thus forming a screening cloud of electrons. The effect of this electron shield on reaction rates depends upon the $\varrho-$ T combination. The thermonuclear reaction rates are enhanced by the electron clouds in stellar interiors and increase over its vacuum value as the barrier penetrability increases due to the decrease of the potential barrier by the screening electron clouds. The multiplication of reaction rates due to electron clouds are important since the energy generation rates and luminosity depend on them.

At low densities and high temperatures the nuclei act as a classical ionized gas, and the effect of the background plasma may be calculated by Debye–Hückel theory. This leads to the "weak screening" approximation, which usually gives a good approximation for higher mass stars, for the reaction rate. For an intermediate regime of ϱ and T, most of the nuclei are bound in a Coulomb lattice structure, but the reacting pair of high energy nuclei is still free. The electrostatic effects are then large, but can still be expressed as a multiplicative factor in the reaction rate, called the "strong screening" correction factor.

Considering a plasma at density ϱ and temperature T it is convenient to introduce the dimensionless parameters Γ and τ.
They are defined as

$$\Gamma = \frac{Z^2 e^2}{akT} \tag{3.24}$$

and

$$\tau = [(\frac{27\pi^2}{4})\frac{M}{kT}\frac{Z^4}{k^2}]^{\frac{1}{3}} \tag{3.25}$$

where

$$a = (\frac{3Z}{4\pi N_e})^{\frac{1}{3}} \tag{3.26}$$

is the mean atomic distance.
Then the state of such a plasma may be characterized by above standard set of dimensionless parameters. Using the numerical values of constants we can rewrite

Γ and τ as

$$\Gamma = 0.22725\frac{Z^2}{T_6}(\frac{\varrho X_A}{A})^{\frac{1}{3}} \tag{3.27}$$

and

$$\tau = 42.48[\frac{Z_1^2 Z_2^2 M_1 M_2}{M_1 + M_2}]^{\frac{1}{3}} T_6^{-\frac{1}{3}}. \tag{3.28}$$

When

$$\Gamma \gg 1$$

the electrostatic energy, E_c, is greater than the thermal energy, kT, the screening becomes strong. The mean atomic distance, a, becomes small which leads that N_e, the number density of electrons, becomes greater. Thus the screening becomes strong in a high−density stellar plasma.

Thus, when

$$\Gamma \ll 1$$

then the electrostatic energy E_c is less than the thermal energy and the screening becomes weak. This takes place in a low−density stellar plasma.

The correct reaction rate in the nuclear reaction can be obtained by multiplying the unscreened rate by a factor f.

$$r_{screened} = f \times r_{unscreened}$$

In high density regime the electrostatic interaction energy between neighboring nuclei becomes large compared to the thermal energies (Γ >kT). The weak screening correction to thermonuclear reaction rates which usually a good approximation for higher mass stars may not hold in the interior of dense low mass stars.

The screening effect of electrons was first considered by Salpeter[26] later improved by other physicists; to mention a few, Salpeter and Van Horn (hereafter SV)[27], Alastuey and Jancovici(hereafter AJ)[28], and IHS[21]. In the present study, the electron screening correction for thermonuclear reaction rates has been calculated using the method formulated by IHS.

Let us first give a brief description of the calculation of screening corrections of above mentioned authors.

i)SV[27]'s work:

The correct thermonuclear reaction rate due to electron screening can be obtained by multiplying the unscreened thermonuclear reaction rate by

$$f_{SV} = exp(-\frac{U_0}{kT}) \tag{3.29}$$

where U_0 is the potential energy term.

Then the weak screening condition is

$$(-\frac{U_0}{kT})_{ws} = 0.188 Z_1 Z_2 \frac{\varrho^{\frac{1}{2}}}{T_6^{\frac{3}{2}}} \xi \tag{3.30}$$

where Z_1, Z_2 are charges of the particles involved in the reaction.

And strong screening condition is given as

$$(-\frac{U_0}{kT})_{ss} = 0.20[(Z_1 + Z_2)^{\frac{5}{3}} - Z_1^{\frac{5}{3}} - Z_2^{\frac{5}{3}}](\frac{\varrho}{\mu})^{\frac{1}{3}}(\frac{1}{T_6}) \tag{3.31}$$

is valid if

$$Z_1 << \varrho^{\frac{1}{3}} \tag{3.32}$$

and

$$(\frac{0.23 Z_1^{\frac{2}{3}}}{T_6}) Z (\frac{\varrho}{\mu})^{\frac{1}{3}} >> 1 \tag{3.33}$$

where T_6 is the temperature $(T/10^6)$, μ is the mean molecular weight.

ii)Method given by AJ[28]:

They studied the enhancement factor of the rate of thermonuclear reaction reactions in dense stellar matter and expressed it in terms of known classical quantities. They stated that in the limiting case of small values of $\frac{3\Gamma}{\tau}$ the enhancement factor can be written as

$$f_{AJ(strong)} = \exp[C - (\frac{45}{32})\frac{\Gamma^3}{\tau^2}]. \tag{3.34}$$

In the case of hydrogen plasma, one can take Γ to be less than 1 (i.e., weak screening).

Hence, above equation is approximated to

$$f_{AJ(weak)} = \exp[C]. \tag{3.35}$$

where

$$C = 1.0531\Gamma + 2.2931\Gamma^{\frac{1}{4}} - 0.5551 \ln \Gamma - 2.35 \tag{3.36}$$

for

$$1 \ll \Gamma \ll 155$$

iii)Method of IHS[21]

IHS have advanced an improved calculation for the enhancement of thermonuclear reaction rates due to strong screening in a dense plasma.
Their calculation was based on the analysis of Monte Carlo computation data for the clasical one−component plasma.
Although the set of calculations of the enhancement factor carried out by SV are based on evaluation of the screening function at zero separation and argued that the classical turning radii for those particals are much smaller than the mean ionic distance, IHS argued that the nuclear reaction rate essentially depends on the probability that the particles tunnel through the repulsive Coulomb barrier. And they investigated the possibility that the correlation function may play a significant part in describing the effects of screening inside the turning radius.
They consider the rate of nuclear reactions in these plasmas in thermodynamic equilibrium at temperature T which are composed of ions and electrons. Then, they stated that the state of such a plasma may be characterized by a standard set of dimensionless parameters given in equations (3.24) and (3.25).
As a result of their calculations IHS gave the enhancement factor due to Coulomb screening as

$$f_{IHS(strong)} = \exp(1.25\Gamma - 0.11\tau(\frac{3\Gamma}{\tau})^2). \tag{3.37}$$

for strong screening. In the domain of weak screening they reach a result for the enhancement factor

$$f_{IHS(weak)} = \exp(3^{\frac{1}{2}}\Gamma^{\frac{3}{2}}) \tag{3.38}$$

Table 3.1: Electron Screening Correction Factors

		SV[27]		AJ[28]		IHS[21]	
Temperature	Density	$f_{1,1}$	$f_{3,3}$	$f_{1,1}$	$f_{3,3}$	$f_{1,1}$	$f_{3,3}$
3.89×10^6	34.8	1.21	2.12	1.35	1.95	1.24	2.34
5.61×10^6	116	1.29	2.80	1.36	2.00	1.25	2.42
6.29×10^6	167	1.23	2.20	1.36	2.01	1.26	2.43
6.59×10^6	205	1.22	2.25	1.37	2.04	1.27	2.48

The calculated screening correction factors and a comparison for the H^1(p, γ)D^2 and He^3(He^3, 2p)He^4 reactions for the set of T and ϱ combinations are given in Table–3.1.

Now, the energy generation rate can be defined as

$$\epsilon_{nuc} = Q \times r_{screened} \qquad \text{erg (gr-sec)}^{-1} \tag{3.39}$$

where Q denotes the energy given off.

The nuclear reaction rates used in the present study are computed according to the expressions given by Fowler et.al. [18] and Harris et.al. [19]. The reaction rate for the first p–p chain H^1(p,$e^+\nu$)D^2 ending with He^3 formation is given by

$$r_{1,1} = 1.02 \times 10^{11} \varrho X_1^2 f_{1,1} g_{1,1} T_6^{-\frac{2}{3}} exp(-33.80 T_6^{-\frac{1}{3}}) \tag{3.40}$$

with

$$g_{1,1} = 1 + 0.0123 T_6^{\frac{1}{3}} + 0.0109 T_6^{\frac{2}{3}} + 9.38 \times 10^{-4} T_6 \tag{3.41}$$

and

$$Q_{1,1} = 1.422 MeV = 2.31 \times 10^{-6} \qquad \text{erg} \tag{3.42}$$

The reaction rate for D^2(p,γ)He^3 reaction is

$$r_{2,1} = 7.38 \times 10^{28} \varrho X_1 X_2 f_{2,1} g_{2,1} T_6^{-\frac{2}{3}} exp(-37.20 T_6^{-\frac{1}{3}}) \tag{3.43}$$

with

$$g_{2,1} = 1 + 0.0112T_6^{\frac{1}{3}} + 0.0199T_6^{\frac{2}{3}} + 0.00156T_6 \tag{3.44}$$

and

$$Q_{2,1} = 5.494MeV = 8.80 \times 10^{-6} \text{ erg} \tag{3.45}$$

The reaction rate for D^2(d,n)He^3 reaction is

$$r_{2,2} = 2.87 \times 10^{33} \varrho X_2^2 f_{2,2} g_{2,2} T_6^{-\frac{2}{3}} exp(-42.58T_6^{-\frac{1}{3}}) \tag{3.46}$$

with

$$g_{2,2} = 1 + 0.0098T_6^{\frac{1}{3}} + 8.76 \times 10^{-3}T_6^{\frac{2}{3}} + 6.00 \times 10^{-4}T_6 \tag{3.47}$$

and

$$Q_{2,2} = 3.269MeV = 5.24 \times 10^{-6} \quad \text{erg} \tag{3.48}$$

The reaction rate for He^3(He^3,2p)He^4 reaction is

$$r_{3,3} = 1.97 \times 10^{35} \varrho X_3^2 f_{3,3} g_{3,3} T_6^{-\frac{2}{3}} exp(-122.76T_6^{-\frac{1}{3}}) \tag{3.49}$$

with

$$g_{3,3} = 1 + 3.40 \times 10^{-3}T_6^{\frac{1}{3}} \tag{3.50}$$

and

$$Q_{3,3} = 12.860MeV = 2.06 \times 10^{-5} \quad \text{erg} \tag{3.51}$$

The reaction rate for $He^3(\alpha,\gamma)Be^7$ reaction is

$$r_{3,4} = 3.85 \times 10^{31} \varrho X_3 X_4 f_{3,4}\, g_{3,4}\, exp[-128.26 T_6^{-\frac{1}{3}} (1 + 4.95 \times 10^{-5}\, T_6)^{\frac{1}{3}}] \quad (3.52)$$

with

$$g_{3,4} = 1 + 3.3 \times 10^{-3} T_6^{\frac{1}{3}} - 3.5 \times 10^{-3} T_6^{\frac{2}{3}} - 8.1 \times 10^{5} T_6 \quad (3.53)$$

and

$$Q_{3,4} = 1.586 MeV = 2.54 \times 10^{-6} \quad \text{erg} \quad (3.54)$$

And, astrophysical cross section factors which correspond to the some of the above reaction rates are as follows:

$S_{1,1}$=3.52×10^{-22} keV−barn,

$S_{3,3}$=5.50×10^{-3} keV−barn,

$S_{3,4}$=0.56 keV−barn.

3.3 Opacity

The opacity used for the model calculations is Los Alamos version of Cox opacity code provided by Eryurt−Ezer[29] which were made avaliable at the Goddard Institute for Space Studies, NASA.

Even though there are some new tables for opacities (Iglesias et. al.[30]),we prefer to use the above mentioned ones since that tables contain line corrections which is important when low temperatures and densities regions over large portion of the stellar structure.

Recently Stother and Chin[31] constructed stellar models using the latest revision of the opacities and concluded that there were surprisingly minor changes from the preliminary stellar models that they published earlier.

The opacity tables were stored in the computer which contains the logarithm of opacity as a function of the logarithm of the temperature and of the logarithm of the density including three hydrogen− helium mixture in which the H−He ratios are 4, 1 and 0. These opacities are useful for the temperature and density combinations of

$$10^{-13} \leq \varrho \leq 10^{5} \qquad \mathrm{gr/cc}$$

$$2 \times 10^{3} \leq T \leq 5.8 \times 10^{8} \qquad \mathrm{K^0}$$

Then the required opacity was obtained by linear interpolation.

CHAPTER IV

RESULTS OF EVOLUTIONARY STUDY

4.1 Overall Results of the Calculations

In the present study, we have studied the pre–main sequence evolution of low mass stars with masses of 0.30, 0.40, 0.50 and 0.60$M_{\odot}$, starting from threshold of stability up to the zero–age main sequence (ZAMS). Also, the main sequence phase of the evolution is partly covered.

The calculations were performed for the chemical composition of X=0.739, Y=0.240, Z=0.021 and for the ratio of mixing length to pressure scale height 1.3 in the construction of the stellar models.

The physical characteristics of the evolutionary models, for stars of our interest, are presented in Tables 4.1–4.4. These are selected among a large number of calculated evolutionary models.

In each of these tables the first column gives the evolutionary time in years, taking the threshold of stability as zero. The second, third, and fourth columns give the radius R and luminosity L of the models in solar units and the logarithm of the corresponding effective temperature T_{eff}. The remaining columns give, in turn, the central density ϱ_c, the central temperature T_c, and the hydrogen abundance by mass X_c at the center of the star. The models indicated by a ' • ' are zero age main sequence (ZAMS) models defined as the model at which the luminosity and the radius attain their lowest value before hydrogen burning phase. The last point in the evolutionary track of all models corresponds to the model at which the hydrogen content at the center has been reduced from

its initial value of 0.739 to $\sim$ 0.600.

The evolutionary paths followed by stars in the mass range 0.30–0.60$M_\odot$ through the phases of gravitational contraction, approach to the main sequence and on the ZAMS are displayed in the theoretical H–R diagram in Figure 4.1.

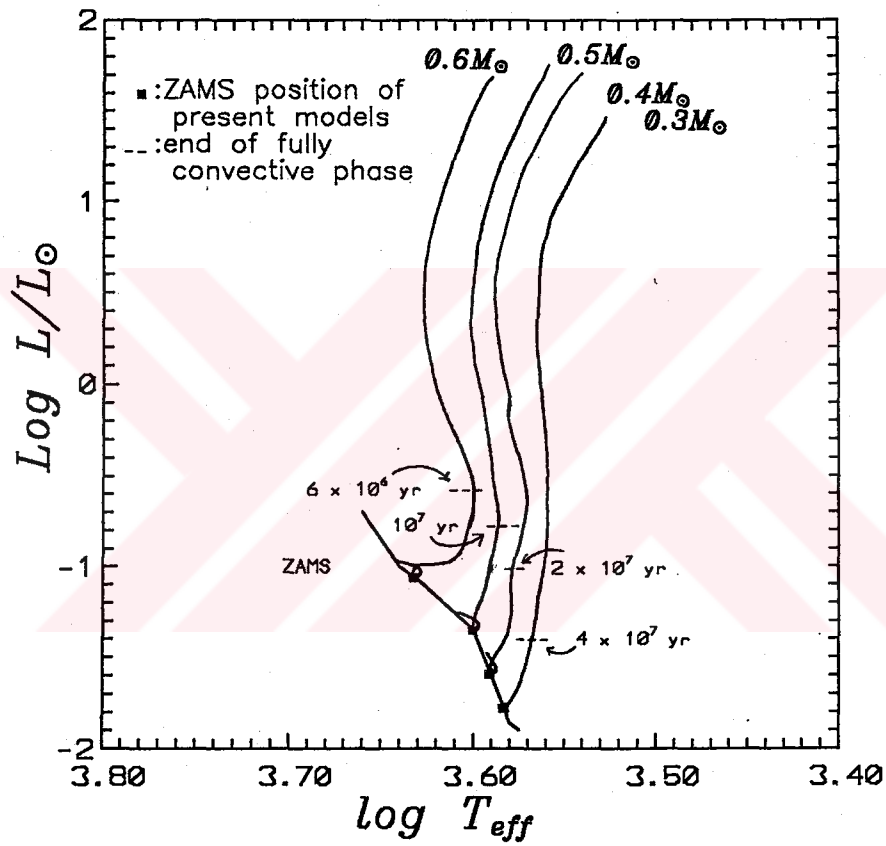

Figure 4.1. The theoretical H–R diagram for the stars of 0.30, 0.40, 0.50, and 0.60 solar masses in the gravitational contraction stage, on the approach to the main sequence, and on the ZAMS.

Figure 4.2 shows the variations of the central temperature and density of low mass stars of indicated masses. In this figure, it is seen that the gas inside the stars in the non–degenerate regime obeys the perfect gas law. Then, it becomes slowly degenerate as star contracts. The central temperature increases with decreasing radius until electron degeneracy begins to set in at which time the central temperature goes through a maximum and then decrease, as it can be seen especially on the path of $0.60M_{\odot}$ star. The limits for perfect gas ($\psi < -4$) and completely degenerate ($\psi > 20$) cases are also shown.

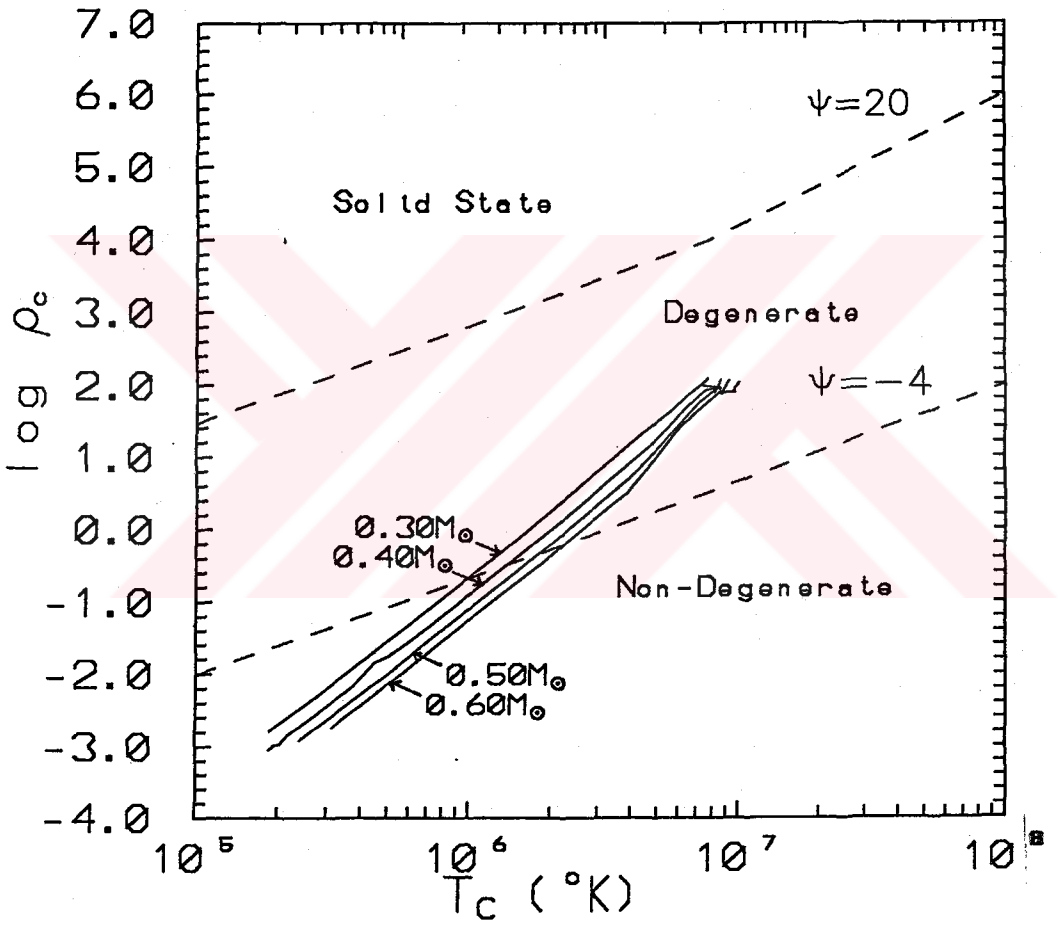

Figure 4.2. The temperature–density diagram for the equation of state and the run of central temperatures and densities for the indicated masses throughout the evolutionary study.

The variations of internal structure of 0.30, 0.40, 0.50, and 0.60 solar masses are displayed in Figure 4.3. Radiative and convective regions are also shown for stars of our interest. For each mass, areas above the curves represent outer convective regions and are displayed in the figure as shaded areas. In each case, the stars are fully convective from the threshold of stability over the almost vertical part of the track down to the point indicated by horizontal dashed lines in Figure 4.1 with an associated evolutionary time. As going from $0.30M_{\odot}$ to $0.60M_{\odot}$ this vertical part and the time the star spends during this phase gets shorter.

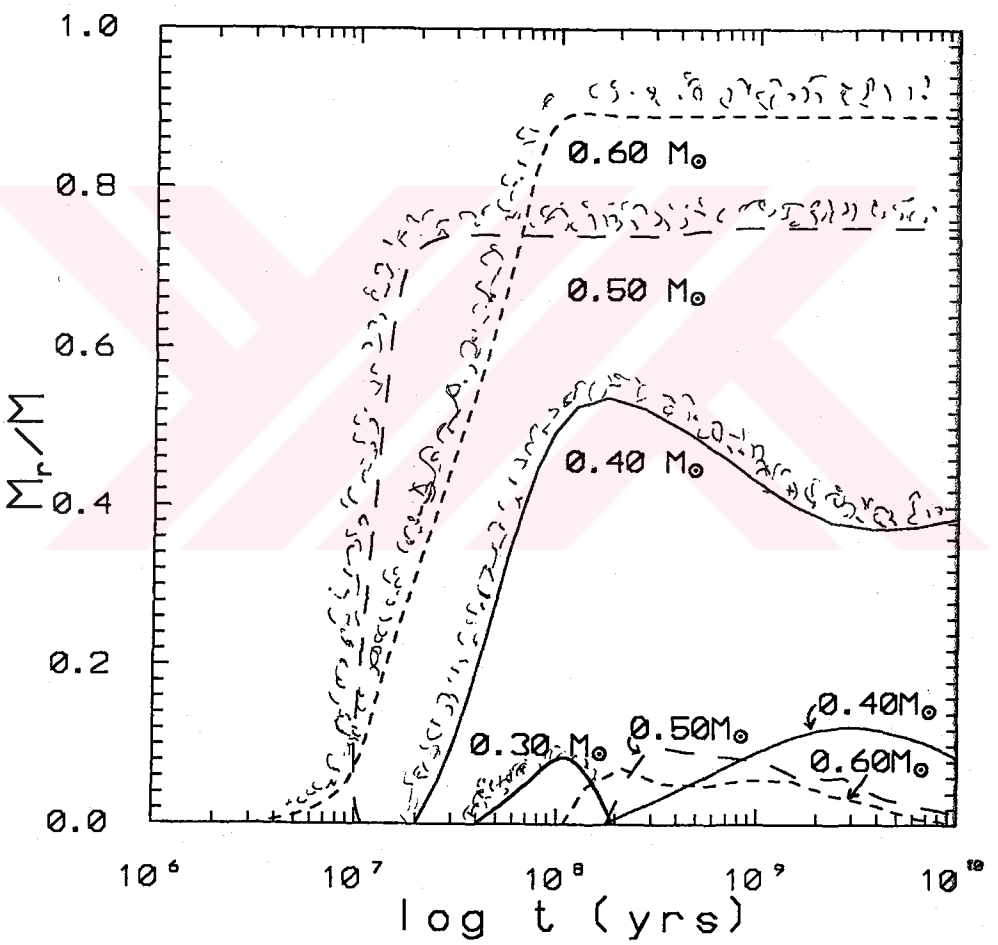

Figure 4.3. The variation of the mass of the outer convective region together with that of convective core for each mass in time.

The wholly convective phase is followed by a radiative phase. In the evolution of $0.40M_{\odot}$ star the radiative core covers, at most, 52% of the mass. In the case of 0.50 and 0.60 solar mass stars the radiative core extends up to 74 % and 88 %, respectively as shown in Figure 4.3.

Thermonuclear energy generation is strong enough to develop a convective core at the center of the 0.40, 0.50 and $0.60M_{\odot}$ stars. These results are shown in Figure 4.3. As seen in this figure the size of the convective core of $0.40M_{\odot}$ star is larger than that of 0.50 and 0.60 solar mass stars. The reason is, probably, the higher exponent (ν) of the proton–proton reactions at lower temperatures ($\epsilon_{pp} \sim T_6^{\nu}$, where ν is decreasing with increasing temperature).

4.1.1 Evolution of $0.30M_{\odot}$ star

The physical characteristics of the model in question are displayed in Table 4.1 and the major results of the evolutionary calculations are shown in Figures 4.3 and 4.4.

The evolutionary path is almost vertical during wholly convective phase. In the given effective temperature at the point of threshold of stability, as the density increases, the surface opacity increases. The increment of opacity prevents the energy flux to increase through the surface layers. Then, the effective temperature remains more or less constant. In fact, the luminosity is governed by the relation $L=4\pi\sigma\ R^2\ T_{eff}^4$ and as the radius decreases the luminosity decreases like $L \sim R^2$. In this way, the star follows a downward part of the track. As seen in Figure 4.3, $0.30M_{\odot}$ star develops a radiative core covering only 7% of the mass after 4×10^7 years. Then, the energy generation produced by nuclear burning becomes great enough to cause the central regions to develop convective instability again. Therefore, it reaches the ZAMS as a wholly convective star at the evolution time of 6.95×10^8 years.

At this stage it has contracted to a radius of $0.28R_{\odot}$. The related luminosity for this radius is $\sim 0.014L_{\odot}$.

Figure 4.4 shows the run of temperature, T/T_c, luminosity, L/L_r, density, ϱ/ϱ_c, radius, r/R, the total nuclear energy, E_N, and change in abundance by mass, X_3 as a function of mass fraction for the $0.30M_{\odot}$ at that time. The scaling factors are $L_r=0.425\times10^{32}$ ergs/s, $T_c=0.73\times10^{7}$, $X_3=0.13\times10^{-2}$, and $E_N=2.8$ erg/g s.

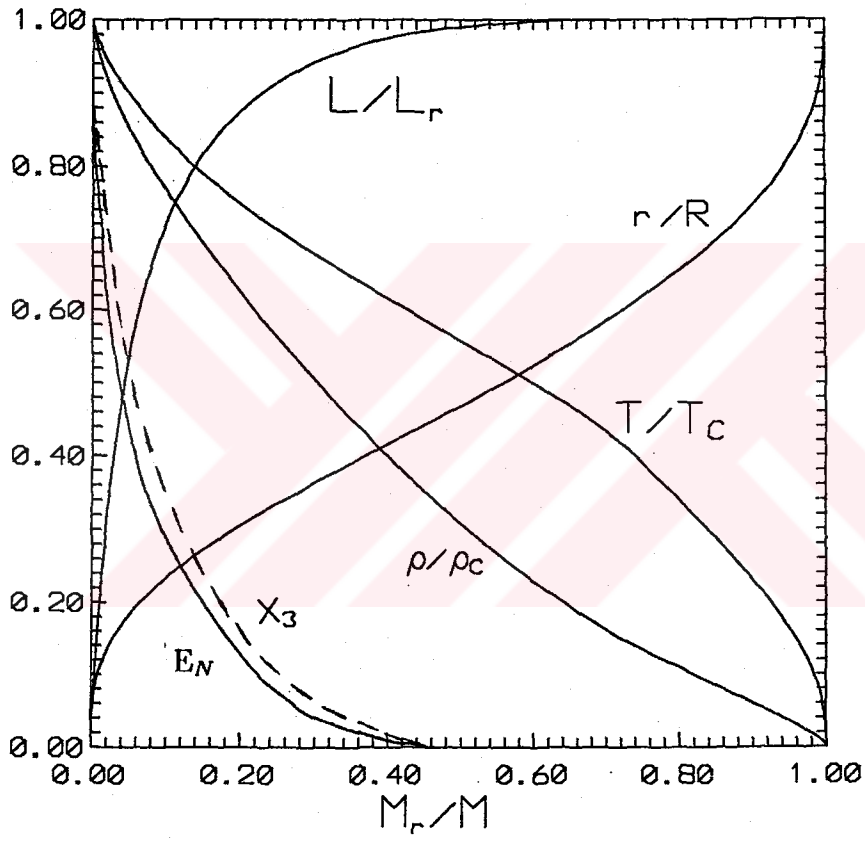

Figure 4.4. The variation of T/T_c, L/L_r, ϱ/ϱ_c, r/R, nuclear energy, E_N, change in abundance by mass, X_3 with mass fraction for the $0.30M_{\odot}$ star on the ZAMS.

4.1.2 Evolution of $0.40M_{\odot}$ star

The evolutionary path of the $0.40M_{\odot}$ star in the theoretical H–R diagram is shown in Figure 4.1. The most part of the path is vertical, similar to the $0.30M_{\odot}$ star.

The wholly convective evolutionary track lasts about 2×10^{7}years when $0.40M_{\odot}$ has a radius of 0.70 $R_{\odot}$ and luminosity of $0.09L_{\odot}$. An increase in the temperature and density at the center of the star begins to develop a radiative core with the rapid decrease of radiation temperature gradient (∇_{rad}) as a result of decrease in opacity. As opacity decreases with increasing of interior temperature and density the luminosity starts to increase and star follows an evolutionary path which is defined by radiative equilibrium. When the star reaches the main sequence in 3.579×10^{8}years, the luminosity attains its minimum value of $0.024L_{\odot}$ at the radius $0.35R_{\odot}$. At this time, the radiative core covers ~52% of the mass of the $0.40M_{\odot}$ star as shown in Figure 4.3. When the energy generated by nuclear burning becomes comparable with gravitational contraction energy He^{3}– He^{3} burning causes the development of the convective core at the center of the star. This convective core covers 13% of the mass of the star.

Figure 4.5 shows the energy produced by the $H^1(p, \beta^+\nu)D^2$ $(p,\gamma)He^3$ (E_{11}) and $He^3(He^3, 2p)He^4$ (E_{33}) reactions, and the change of abundance by mass of He^3 at the center of the $0.40M_\odot$ star with time. The scaling factors are E_{11s}=3.2 erg/g s, E_{33s}=3.1 erg/g s, $X_3=3.20\times10^{-3}$,

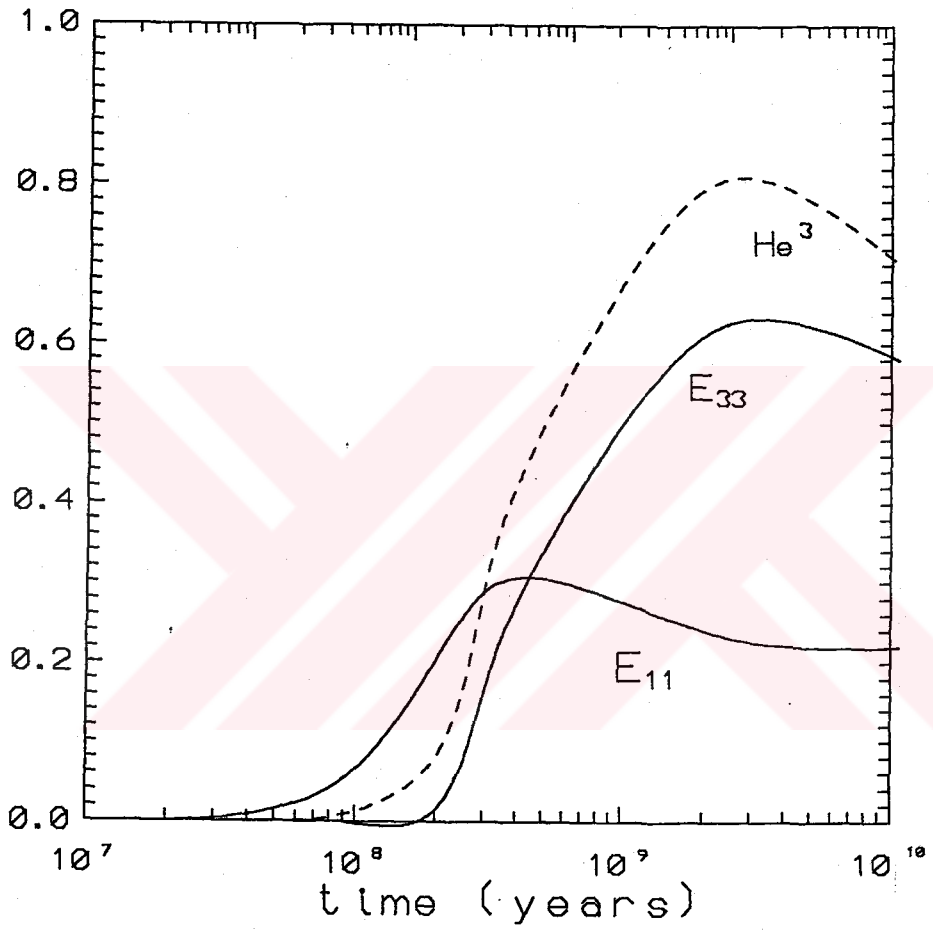

Figure 4.5. The energy produced by the first two p−p and He^3− He^3 reactions and the change of abundance by mass of He^3 at the center of the $0.40M_\odot$ star with time.

He^3 begins to form at the central temperature of about 5.42×10^6 K^0 and central density 25.1 gm/cc after 4.8×10^7 years of evolution. The abundance of X^3 keeps increasing toward the surface of the star. After 3×10^9 yr, C^{12} starts to contribute to energy generation of the star when convective core reaches its maximum value.

In Figure 4.6, the distribution of temperature, luminosity, radius, density, the total nuclear energy E_N and He^3 abundance by mass are presented as a function of mass fraction throughout the interior of $0.40M_\odot$ star at the evolution time of ZAMS. The scaling factors are $L_r=1.06\times10^{32}$ ergs/s, $T_c=7.48\times10^6$ K^0, $X_3=1.78\times10^{-4}$, $E_N=0.55$ erg/g s and $\varrho_c=78$ gm/cc.

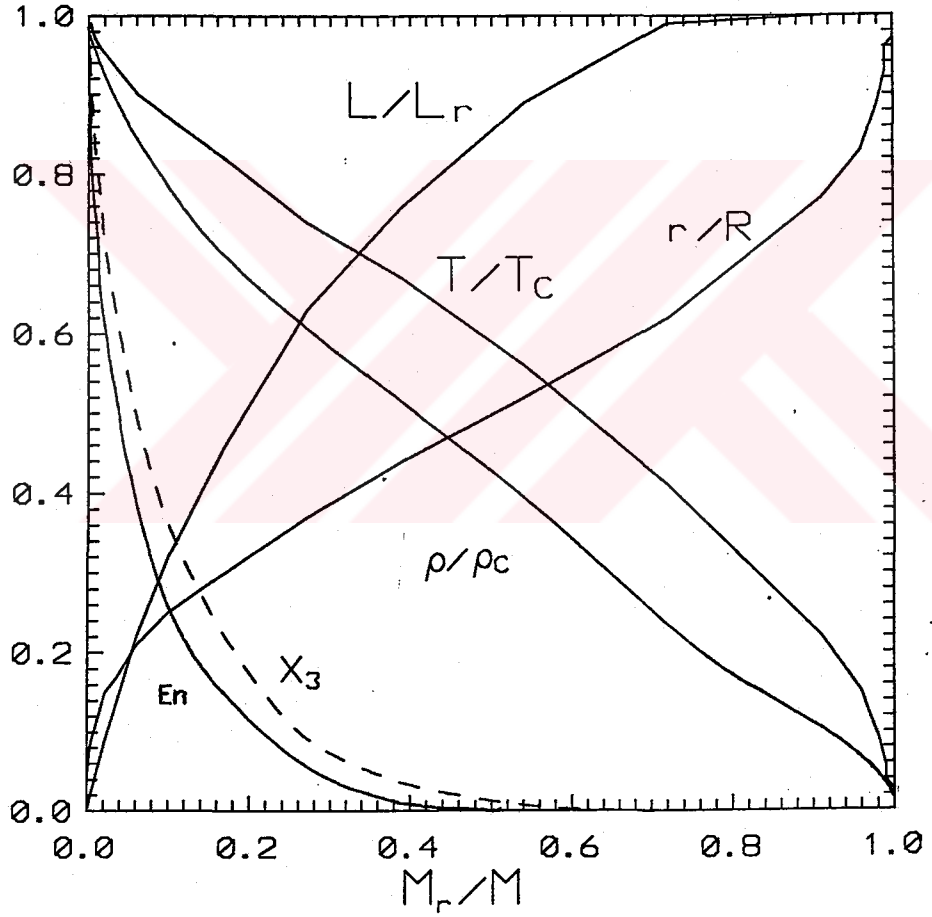

Figure 4.6. The variation with mass fraction of the variables Temperature, Luminosity, Radius, Density, E_N, and He^3 abundance by mass for the $0.40M_\odot$ star at the model on the ZAMS.

4.1.3 Evolution of 0.50 and 0.60$M_\odot$ stars

The physical characteristics of the evolutinary models for stars of 0.50 and 0.60 solar mass are given, respectively, in tables 4.3 and 4.4. The wholly convective evolutionary track lasts about 10^7years for 0.50$M_\odot$ and about 6×10^6years for 0.60$M_\odot$. Then the radiative core starts to develop at the center of the star. This radiative core never covers more than 74% of the 0.50$M_\odot$ star and 88% of the 0.60$M_\odot$ star.

In the evolution of 0.60$M_\odot$ star, with the increase of central temperature and density the reactions forming He^3 start to contribute to the flow of the total energy and the He^3 abundance reaches its equilibrium value in about 10^9years. The energy generated by formation of the He^3 is strong enough to cause the development of a convective core at the center of the star. This convective core covers about 8% of the mass and entirely disappears at 8×10^9years. As He^3 is consumed sufficiently, the convective core recedes. Second increase in the size of the convective core is due to the rising central temperatures and densities.

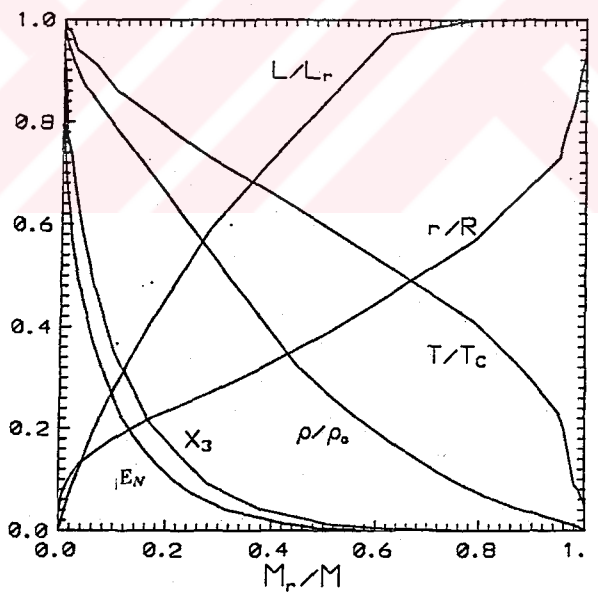

Figure 4.7. The variation with mass fraction of the variables Temperature, Density, Luminosity, Radius, He^3 abundance by mass and E_N for the 0.60$M_\odot$ star at the model on the ZAMS.

The distribution of temperature (T/T_c), density (ϱ/ϱ_c), luminosity (L/L_r), radius (r/R), He^3 abundance by mass (X_3) and the total energy generation (E_N) are displayed in Figure 4.7 as a function of mass fraction in the interior of the star at the ZAMS state.

Inside the convective core He^3 and C^{12} are in an average equilibrium in which the total rates of formation and destruction throughout the core are equal. In the evolution of 0.50 solar mass, He^3 reaches its equilibrium abundance in 10^8years. Then, a convective core develops at the center of the star and reduces the contribution of the gravitational energy to the total energy output of the star, resulting in a decline in luminosity. The central convective core covers only 9% of the total mass.

4.2 Comparison of the present results with other Theoretical Stellar Models and Observations

i)Comparison with other recent theoretical stellar models:

The properties of the previous stellar models over a mass range 0.30 to 0.60 solar masses in the ZAMS phase have displayed in Table 4.5. This table includes our own results and that of authors who are all mentioned in Chapter I. The columns 3−5 and 6−7 represent the surface and center parameters for the ZAMS models, respectively. The models that were selected have initial chemical compositions almost similar to that used in this study. Comparison of the present results with previous calculated models for stars in the mass range of interest shows a good agreement between the ZAMS of the present study and those of CJJ.

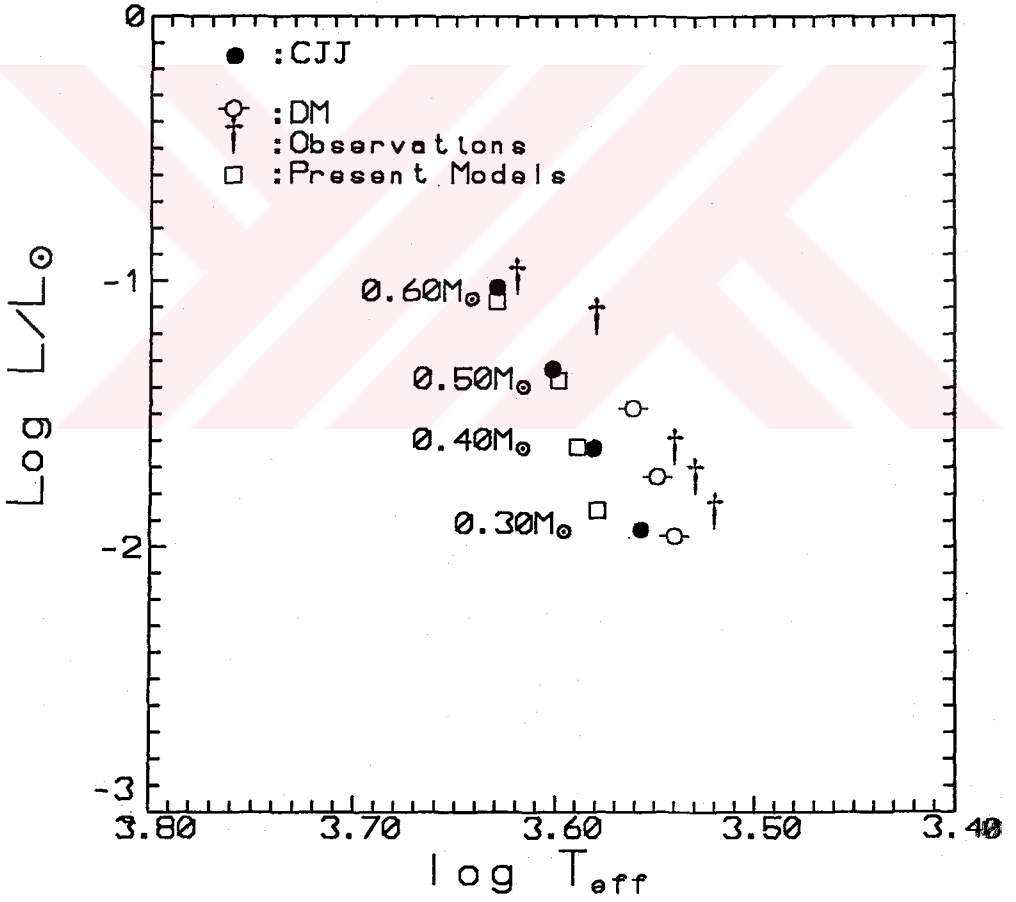

Figure 4.8. Comparison of theoretical model results for stars of our interest.

The luminosities of present models are higher than DM models. Both CJJ and DM models together with present ones show that 0.30 solar mass star to be completely convective on the ZAMS. We have found central temperature, T_c, to be equivalent while central densities, ϱ_c, are higher for $0.30M_\odot$ star. For 0.40 and 0.50 solar mass stars the central densities are found to be lower as compared with CJJ models. For $0.60M_\odot$ central density is comparable with CJJ model.

The comparison is displayed in the theoretical H−R diagram in Figure 4.8. The differences arising from above mentioned ones and other theoretical works are mainly due to implementation of the different input physics. For instance, the change in the mixing length parameter causes a shift in the position of the star in the H−R diagram. As the mixing length parameter decreases, the position of the star shifts towards lower−right from the previous position. The results of the previous models mentioned in Table 4.5 are obtained by using more or less the same mixing length parameter, which is 1. While present models were performed by using a value of 1.3. Besides this, the helium abundance used in this study is lower than previous ones, $\sim \Delta Y = 0.04$. Opacities used in the evolutionary calculations are also different.

ii)Comparison with Observations:

The best way to check stellar evolution calculations is, of course, to compare calculated evolutionary tracks with observed ones. In order to compare theoretical stellar models with the observed low mass stars the following data must be known for a given star:

1.mass

2.luminosity

3.effective temperature (or radius)

The knowledge of the last two quantities allow the star to be placed in the H−R diagram and, with the knowledge of the mass of the star, a mass calibration for the main sequence can be established.

The measurement of stellar masses is one of the difficult observational

problems in astronomy. In order to determine the mass of a star it must be a member of a binary system. Then, substantial information concerning the properties of LMS stars can be obtained from the observations of visual, spectroscopically resolved, and eclipsing binaries. These binaries provide the data necessary to obtain the relationship between the mass and luminosity of low mass stars since the masses of the components of these systems can be directly determined.

In Table–4.6, we list the observational properties of low mass stars in binary systems for the mass range of $0.30–0.60M_{\odot}$. The theoretical and observational luminosity–mass relation are shown in Figure 4.9. The observational points including error estimates are taken from Popper[32]. These stars are all main sequence stars having spactral types ranging from M to K. As seen in this figure a good agreement exists for stars namely Kr 60 A, Wolf 630, YY Gem A,B and HR 6426 B. They have masses of 0.28, 0.42, 0.59 and $0.54M_{\odot}$, respectively, with the probable errors in mass as indicated in Table–4.6. We obtained a good fit with $0.30M_{\odot}$ for Kr 60 A, $0.40M_{\odot}$ for Wolf 630 and $0.60M_{\odot}$ for YY Gem A, B and HR 6426 B.

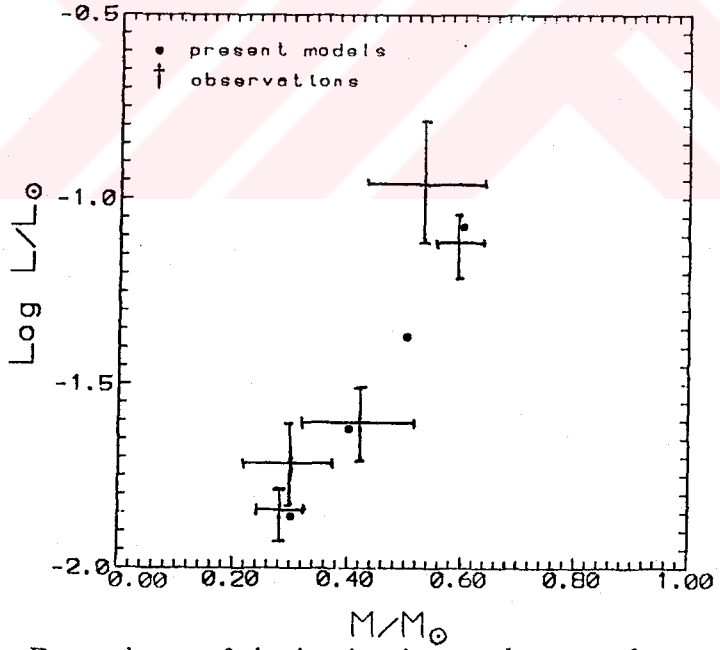

Figure 4.9. Dependence of the luminosity on the mass for present models. The observation points including error estimates are from Popper[32].

Figure 4.10 represents the comparison of the results of the present work with the position of observed low mass stars. The best that we can do for comparison of observed low mass stars with the present results is to define a region in the H−R diagram centered on the points of log T_{eff} and log $L/L_{\odot}$ with errors Δlog T_{eff} and Δlog $L/L_{\odot}$.

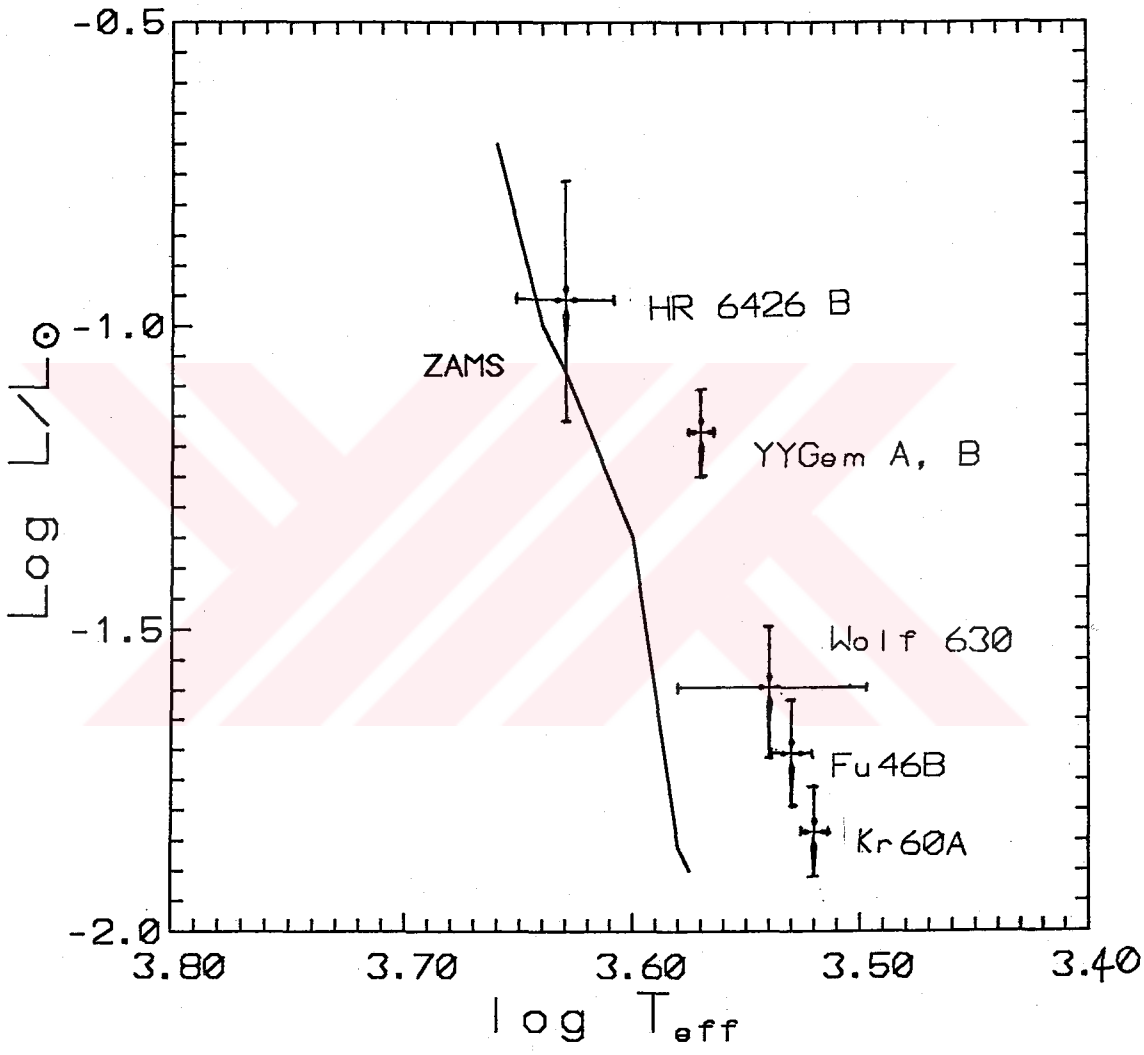

Figure 4.10. The ZAMS of present models and a comparison with observed low mass stars in the H−R diagram.

All of these observed low mass stars under consideration have lower effective temperature than present ones, except Wolf 630. Kr 60 A and Wolf 630 have almost the same luminosity as compared with the position of $0.30M_{\odot}$ and $0.40M_{\odot}$ stars, respectively. The difference is $\Delta\log T_{eff}=0.049$, in the H−R diagram with probable observational error of $\Delta\log T_{eff}=\mp 0.017$, for Wolf 630. But HR 6426 B can be settled on a region in the H−R diagram centered on the point $\log T_{eff}=3.62$ and $\log L/L_{\odot}=-0.98$ with sides $\Delta\log T_{eff}=0.028$ and $\Delta\log L/L_{\odot}=0.196$ as shown in the Figure 4.10. This indicates that a good agreement is obtained for the observation of HR 6426 B with $0.60M_{\odot}$. Then the following conclusions can be drawn:

HR 6426 B is a star approaching to ZAMS having an age of $\sim 1.08\times 10^{8}$yr at a radius of $0.56R_{\odot}$. The centeral temperature and density corresponding this time are around 9×10^{6} Kelvin degrees and 78 gr/cc, respectively.

Table 4.7 represents the distribution with mass fraction of temperature, density, radius and luminosity of the model corresponding to HR 6426 B at the evolution time $\sim$ t=1.08×10^{8}yr. These results are also displayed on Figure 4.11.

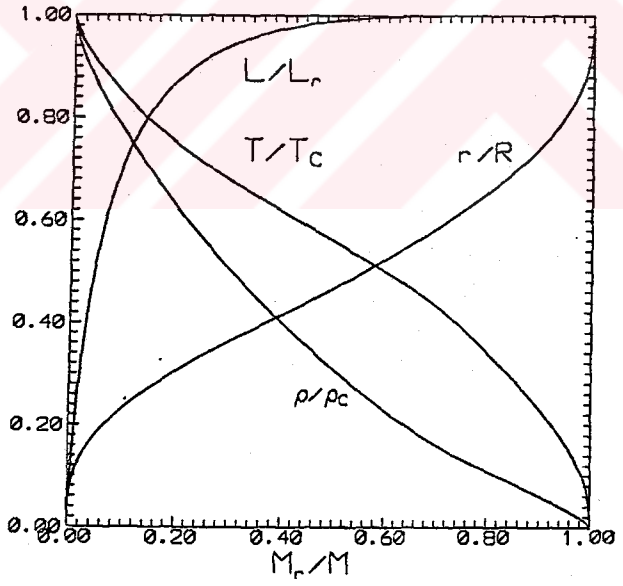

Figure 4.11. The distribution with mass fraction of temperature, density, radius, luminosity of the model corresponding to HR 6426 B at the evolution time $\sim$ t=1.08×10^{8}yr.

As seen in the Figure 4.8 that for masses higher than $0.50M_{\odot}$ the present results show the same path with the observed stars. But below this limit there is a separation. Dissagreement of the position of observed low mass stars, except the one mentioned above, in H−R diagram is due to the effects explained in section 4.2.

Other observational candidates for pre−main sequence stars are those of T Tauri stars which are perhaps the most relevant sample of objects because, they have been accepted as stars still in the pre− main sequence gravitational contraction phase of stellar evolution. In Figure 4.12 we have plotted the positions in the H−R diagram of the T Tauri stars belonging to the Taurus−Auriga Molecular Cloud Complex, Stahler[33]. Also shown are the evolutionary tracks of present models. They are all collected around 0.30, 0.40 and 0.50 solar mass stars.

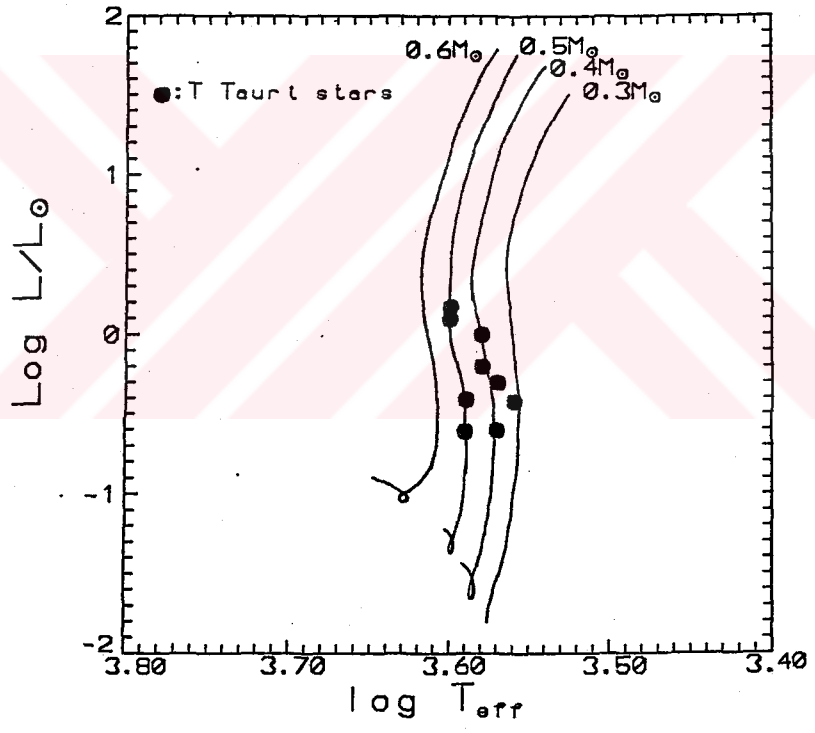

Figure 4.12. The theoretical H−R diagram for the stars having 0.30, 0.40, 0.50, and 0.60 solar masses and a comparison with observational H−R diagram of Taurus−Auriga Molecular Cloud Complex. • 's represent the T Tauri observations (Stahler[33]).

The results of our theoretical evolutionary study of stars of our interest enable us to draw theoretical lines of equal age in the H−R diagram by joining the points corresponding to the same evolutionary time on the tracks of each mass. In Figure 4.13 the isochrones for t=10^5yr, t=10^6yr and t=6×10^6yr are dispayed and compared with the positions of T Tauri stars in that diagram.
The upper limit to the ages of the sample seems to be about 6×10^6yr which is in agreement with the estimates of $\sim5\times10^6$yr by Herbig[34].

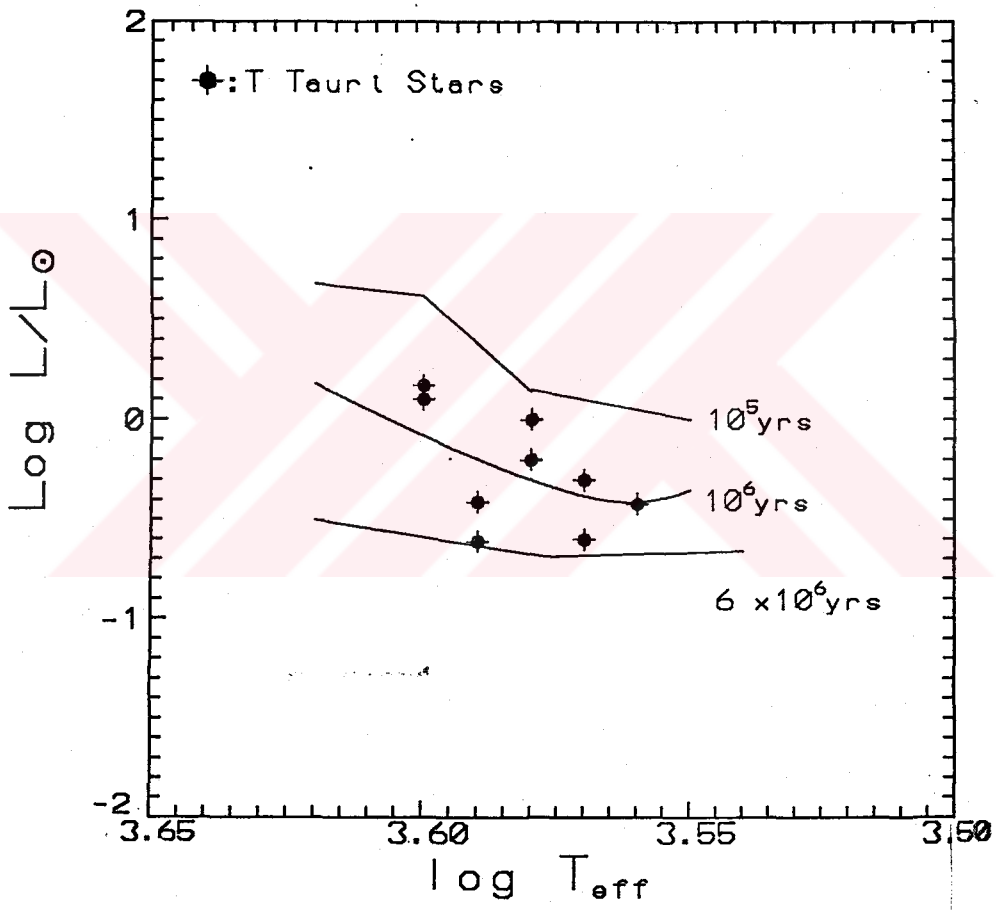

Figure 4.13. The theoretical time lines and the observed H−R diagram for T Tauri stars in Taurus Auriga Molecular Cloud Complex.

Table 4.1: The evolutionary sequence of models for M = 0.30 $M_\odot$

	time(yrs)	$R/R_\odot$	$L/L_\odot$	log T_e	ϱ_c	T_c	X_c
	5.000×10^{0}	1.46×10^{1}	2.55×10^{1}	3.54	1.63×10^{-3}	1.86×10^{5}	0.739
	1.500×10^{1}	1.45×10^{1}	2.58×10^{1}	3.54	1.64×10^{-3}	1.87×10^{5}	0.739
	3.150×10^{2}	1.34×10^{1}	2.22×10^{1}	3.54	2.03×10^{-3}	2.01×10^{5}	0.739
	5.115×10^{3}	8.86×10^{0}	1.12×10^{1}	3.55	5.86×10^{-3}	2.61×10^{5}	0.739
	1.024×10^{4}	7.48×10^{0}	8.24×10^{0}	3.56	9.19×10^{-3}	3.39×10^{5}	0.739
	6.144×10^{4}	4.12×10^{0}	2.75×10^{0}	3.57	4.68×10^{-2}	5.91×10^{5}	0.739
	1.024×10^{5}	3.40×10^{0}	1.90×10^{0}	3.57	8.00×10^{-2}	7.09×10^{5}	0.739
	6.758×10^{5}	1.92×10^{0}	5.53×10^{-1}	3.56	4.09×10^{-1}	1.23×10^{6}	0.739
	2.970×10^{6}	1.15×10^{0}	2.03×10^{-1}	3.56	1.81×10^{0}	1.99×10^{6}	0.739
	5.591×10^{6}	9.51×10^{-1}	1.41×10^{-1}	3.56	3.16×10^{0}	2.37×10^{6}	0.739
	8.212×10^{6}	8.06×10^{-1}	1.03×10^{-1}	3.56	5.12×10^{0}	2.77×10^{6}	0.739
	4.491×10^{7}	4.62×10^{-1}	3.68×10^{-2}	3.57	2.66×10^{1}	4.73×10^{6}	0.739
	1.078×10^{8}	3.29×10^{-1}	1.92×10^{-2}	3.58	7.34×10^{1}	6.46×10^{6}	0.739
	3.595×10^{8}	2.79×10^{-1}	1.40×10^{-2}	3.58	1.20×10^{2}	7.58×10^{6}	0.739
•	6.950×10^{8}	2.76×10^{-1}	1.38×10^{-2}	3.58	1.23×10^{2}	7.65×10^{6}	0.738
	1.366×10^{9}	2.77×10^{-1}	1.39×10^{-2}	3.58	1.22×10^{2}	7.62×10^{6}	0.737
	2.708×10^{9}	2.82×10^{-1}	1.44×10^{-2}	3.58	1.15×10^{2}	7.51×10^{6}	0.736
	5.393×10^{9}	2.90×10^{-1}	1.51×10^{-2}	3.58	1.07×10^{2}	7.34×10^{6}	0.734
	1.076×10^{10}	2.93×10^{-1}	1.53×10^{-2}	3.58	1.03×10^{2}	7.29×10^{6}	0.731
	4.297×10^{10}	2.97×10^{-1}	1.59×10^{-2}	3.58	9.90×10^{1}	7.30×10^{6}	0.713
	6.445×10^{10}	2.98×10^{-1}	1.61×10^{-2}	3.58	9.80×10^{1}	7.34×10^{6}	0.702
	3.211×10^{11}	3.03×10^{-1}	1.82×10^{-2}	3.59	9.40×10^{1}	8.17×10^{6}	0.567

•ZAMS values

Table 4.2: The evolutionary sequence of models for M = 0.40 $M_\odot$

	time(yrs)	$R/R_\odot$	$L/L_\odot$	log T_e	ϱ_c	T_c	X_c
	5.000×10^{0}	1.93×10^{1}	4.87×10^{1}	3.54	8.98×10^{-4}	1.85×10^{5}	0.739
	1.500×10^{1}	1.92×10^{1}	4.79×10^{1}	3.54	9.20×10^{-4}	1.86×10^{5}	0.739
	3.150×10^{2}	1.73×10^{1}	4.13×10^{1}	3.55	1.19×10^{-3}	2.04×10^{5}	0.739
	5.115×10^{3}	1.08×10^{1}	1.88×10^{1}	3.57	4.11×10^{-3}	3.13×10^{5}	0.739
	1.024×10^{4}	8.99×10^{0}	1.37×10^{1}	3.57	6.72×10^{-3}	3.70×10^{5}	0.739
	2.150×10^{5}	2.87×10^{0}	1.72×10^{0}	3.59	1.55×10^{-1}	1.09×10^{6}	0.739
	6.605×10^{6}	9.82×10^{-1}	2.06×10^{-1}	3.57	2.77×10^{0}	3.05×10^{6}	0.739
	2.233×10^{7}	6.81×10^{-1}	8.31×10^{-2}	3.58	1.12×10^{1}	4.34×10^{6}	0.739
	4.330×10^{7}	5.58×10^{-1}	7.32×10^{-2}	3.58	1.37×10^{1}	5.16×10^{6}	0.739
	6.428×10^{7}	4.75×10^{-1}	4.26×10^{-2}	3.58	3.63×10^{1}	5.92×10^{6}	0.739
	1.062×10^{8}	4.05×10^{-1}	3.64×10^{-2}	3.59	4.79×10^{1}	6.84×10^{6}	0.739
	1.901×10^{8}	3.62×10^{-1}	2.71×10^{-2}	3.59	8.51×10^{1}	7.75×10^{6}	0.739
•	3.579×10^{8}	3.49×10^{-1}	2.39×10^{-2}	3.59	7.80×10^{1}	8.22×10^{6}	0.738
	6.934×10^{8}	3.54×10^{-1}	2.44×10^{-2}	3.59	7.83×10^{1}	8.14×10^{6}	0.735
	2.707×10^{9}	3.57×10^{-1}	2.45×10^{-2}	3.59	7.84×10^{1}	8.11×10^{6}	0.728
	5.391×10^{9}	3.60×10^{-1}	2.51×10^{-2}	3.59	7.88×10^{1}	8.09×10^{6}	0.717
	1.076×10^{10}	3.62×10^{-1}	2.54×10^{-2}	3.59	8.07×10^{1}	8.12×10^{6}	0.696

•ZAMS values

Table 4.3: The evolutionary sequence of models for M = 0.50 $M_\odot$

	time(yrs)	$R/R_\odot$	$L/L_\odot$	log T_e	ϱ_c	T_c	X_c
	5.000×10^{0}	1.79×10^{1}	4.88×10^{1}	3.56	1.21×10^{-3}	2.40×10^{5}	0.739
	1.550×10^{2}	1.73×10^{1}	4.58×10^{1}	3.56	1.34×10^{-3}	2.49×10^{5}	0.739
	1.275×10^{3}	1.46×10^{1}	3.54×10^{1}	3.57	2.10×10^{-3}	2.90×10^{5}	0.739
	5.115×10^{3}	1.14×10^{1}	2.31×10^{1}	3.58	4.12×10^{-3}	3.65×10^{5}	0.739
	1.024×10^{4}	9.62×10^{0}	1.76×10^{1}	3.58	6.49×10^{-3}	4.25×10^{5}	0.739
	4.096×10^{4}	6.41×10^{0}	8.48×10^{0}	3.58	2.00×10^{-2}	6.22×10^{6}	0.739
	1.024×10^{5}	4.31×10^{0}	4.20×10^{0}	3.60	6.18×10^{-2}	9.09×10^{5}	0.739
	6.758×10^{5}	2.35×10^{0}	1.24×10^{0}	3.60	3.59×10^{-1}	1.64×10^{6}	0.739
	2.132×10^{7}	7.88×10^{-1}	1.22×10^{0}	3.59	9.32×10^{0}	4.60×10^{6}	0.739
	3.181×10^{7}	6.72×10^{-1}	8.81×10^{-2}	3.59	1.62×10^{1}	5.27×10^{6}	0.739
	1.786×10^{8}	4.55×10^{-1}	4.67×10^{-2}	3.60	9.44×10^{1}	8.39×10^{6}	0.739
•	3.464×10^{8}	4.42×10^{-1}	4.24×10^{-2}	3.60	7.31×10^{1}	8.62×10^{6}	0.737
	5.547×10^{9}	4.46×10^{-1}	4.36×10^{-2}	3.60	8.16×10^{1}	8.70×10^{6}	0.703
	8.232×10^{9}	4.48×10^{-1}	4.43×10^{-2}	3.60	8.44×10^{1}	8.74×10^{6}	0.683
	1.092×10^{10}	4.51×10^{-1}	4.50×10^{-2}	3.60	8.74×10^{1}	8.78×10^{6}	0.661
	1.628×10^{10}	4.56×10^{-1}	4.64×10^{-2}	3.60	9.45×10^{1}	8.88×10^{6}	0.615

•ZAMS values

Table 4.4: The evolutionary sequence of models for M = 0.60 $M_\odot$

time(yrs)	$R/R_\odot$	$L/L_\odot$	log T_e	ϱ_c	T_c	X_c
5.000×10^{0}	1.60×10^{1}	5.11×10^{1}	3.58	1.83×10^{-3}	3.13×10^{5}	0.739
1.550×10^{2}	1.56×10^{1}	4.23×10^{1}	3.57	1.95×10^{-3}	3.20×10^{5}	0.739
1.275×10^{3}	1.39×10^{1}	3.62×10^{1}	3.58	2.67×10^{-3}	3.56×10^{5}	0.739
5.115×10^{3}	1.14×10^{1}	2.56×10^{1}	3.59	4.61×10^{-3}	4.28×10^{5}	0.739
1.024×10^{4}	9.87×10^{0}	2.02×10^{1}	3.59	6.88×10^{-3}	4.90×10^{5}	0.739
1.229×10^{5}	4.45×10^{0}	4.98×10^{0}	3.61	6.60×10^{-2}	1.05×10^{6}	0.739
6.758×10^{5}	2.35×10^{0}	1.24×10^{0}	3.60	3.59×10^{-1}	1.64×10^{6}	0.739
1.352×10^{6}	2.01×10^{0}	1.01×10^{0}	3.61	6.70×10^{-1}	2.28×10^{6}	0.739
1.118×10^{7}	9.89×10^{-1}	2.09×10^{-1}	3.60	5.75×10^{0}	4.38×10^{6}	0.739
2.167×10^{7}	8.32×10^{-1}	1.49×10^{-1}	3.60	1.09×10^{1}	5.08×10^{6}	0.739
1.056×10^{8}	5.92×10^{-1}	9.81×10^{-2}	3.63	7.74×10^{1}	8.38×10^{6}	0.739
1.894×10^{8}	5.46×10^{-1}	8.41×10^{-2}	3.63	7.92×10^{1}	9.51×10^{6}	0.738
3.461×10^{9}	5.47×10^{-1}	8.34×10^{-2}	3.62	8.47×10^{1}	9.55×10^{6}	0.687
4.132×10^{9}	5.48×10^{-1}	8.41×10^{-2}	3.63	8.62×10^{1}	9.57×10^{6}	0.677
1.017×10^{10}	5.59×10^{-1}	9.08×10^{-2}	3.63	9.96×10^{1}	9.79×10^{6}	0.589

•ZAMS values

Table 4.5: Comparison of Theoretical Models for Various Masses*

	Authors	$\log L/L_\odot$	$\log T_{eff}$	$R/R_\odot$	$\log T_c$	$\log \varrho_c$
	CJJ[3](0.70, 0.02)	-1.931	3.557	0.281	6.884	1.979
	GHG[5](0.68, 0.03)	-2.050	3.510	0.302	6.874	1.981
	Sien[6](0.70, 0.03)	-1.996	3.528	0.293	6.880	1.999
$M=0.30M_\odot$	VHDA[7](0.73, 0.02)	-2.012	3.528	0.288	6.869	2.018
	Neece[9](0.68, 0.03)	-2.045	3.492	0.330	6.883	2.005
	DM[10](0.73, 0.02)	-1.956	3.540	0.291	6.866	2.050
	NRJ[11](0.70, 0.02)	-1.959	3.549	0.280	6.890	2.053
	Present(0.739, 0.021)	-1.860	3.579	0.276	6.884	2.089
	CJJ[3](0.70, 0.02)	-1.628	3.581	0.356	6.918	1.938
	GHG[5](0.68, 0.03)	-1.744	3.528	0.394	6.913	1.982
$M=0.40M_\odot$	VHDA[7](0.73, 0.02)	-1.726	3.540	0.365	6.900	1.910
	Neece[9](0.68, 0.03)	-1.708	3.526	0.415	6.928	1.999
	DM[10](0.73, 0.02)	-1.734	3.549	0.361	6.902	1.934
	Present(0.739, 0.021)	-1.622	3.589	0.350	6.914	1.892
	CJJ[3](0.70, 0.02)	-1.330	3.602	0.454	6.954	1.945
	GHG[5](0.68, 0.03)	-1.430	3.546	0.521	6.957	1.994
$M=0.50M_\odot$	Neece[9](0.68, 0.03)	-1.397	3.563	0.502	6.972	1.990
	DM[10](0.73, 0.02)	-1.477	3.561	0.459	6.936	1.921
	Present(0.739, 0.021)	-1.372	3.599	0.450	6.932	1.903
	VHDA[7](0.73, 0.02)	-1.172	3.594		6.969	1.898
$M=0.60M_\odot$	CJJ[3](0.70, 0.02)	-1.024	3.630	0.568	6.996	1.960
	Present(0.739, 0.021)	-1.075	3.630	0.546	6.978	1.899

*Author abbrevations are the same explained in the text.
After each author abbrevation, the numbers in parenthesis represent chemical composition:(X, Z).

Table 4.6: Properties of some observed low mass stars

Name	$M/M_{\odot} \mp \Delta^*$	$\log T_{eff} \mp \Delta^*$	$\log L/L_{\odot} \mp \Delta^*$
Kr60A**	0.28∓0.03	3.52∓0.005	-1.86∓0.068
Fu46B**	0.30∓0.07	3.53∓0.012	-1.73∓0.102
Wolf 630**	0.42∓0.10	3.54∓0.017	-1.62∓0.104
HR 6426 B**	0.54∓0.10	3.62∓0.028	-0.98∓0.196
YYGem A, B**	0.59∓0.02	3.58∓0.003	-1.13∓0.102

*Δ's represent the errors.

**DNC[12], Popper[32].

Table 4.7: The variation of physical parameters of the model corresponding to HR 6426 B at the evolution time $\sim 1.08\times10^{8}$yr.

M_r/M	r/R	ϱ/ϱ_c	T/T_c	L_r/L
0	0	1	1	0
5.000×10^{-4}	3.786×10^{-2}	9.930×10^{-1}	9.953×10^{-1}	1.347×10^{-2}
1.007×10^{-3}	4.788×10^{-2}	9.889×10^{-1}	9.926×10^{-1}	2.555×10^{-2}
4.086×10^{-3}	7.665×10^{-2}	9.719×10^{-1}	9.812×10^{-1}	8.907×10^{-2}
7.446×10^{-3}	9.390×10^{-2}	9.582×10^{-1}	9.719×10^{-1}	1.471×10^{-1}
1.005×10^{-2}	1.039×10^{-1}	9.489×10^{-1}	9.657×10^{-1}	1.867×10^{-1}
4.504×10^{-2}	1.747×10^{-1}	8.622×10^{-1}	9.060×10^{-1}	5.069×10^{-1}
7.427×10^{-2}	2.089×10^{-1}	8.085×10^{-1}	8.679×10^{-1}	6.417×10^{-1}
1.002×10^{-1}	2.333×10^{-1}	7.664×10^{-1}	8.378×10^{-1}	7.202×10^{-1}
3.307×10^{-1}	3.791×10^{-1}	4.707×10^{-1}	6.585×10^{-1}	9.547×10^{-1}
6.169×10^{-1}	5.333×10^{-1}	2.162×10^{-1}	4.885×10^{-1}	9.976×10^{-1}
8.327×10^{-1}	6.815×10^{-1}	9.332×10^{-2}	3.062×10^{-1}	9.998×10^{-1}
9.592×10^{-1}	8.229×10^{-1}	3.059×10^{-2}	1.487×10^{-1}	9.999×10^{-1}
9.677×10^{-1}	8.387×10^{-1}	2.578×10^{-2}	1.339×10^{-1}	1
9.725×10^{-1}	8.485×10^{-1}	2.301×10^{-2}	1.250×10^{-1}	1
9.818×10^{-1}	8.714×10^{-1}	1.717×10^{-2}	1.047×10^{-1}	1
9.932×10^{-1}	9.121×10^{-1}	8.776×10^{-3}	6.998×10^{-2}	1
9.965×10^{-1}	9.319×10^{-1}	5.606×10^{-3}	5.340×10^{-2}	1
9.981×10^{-1}	9.463×10^{-1}	3.697×10^{-3}	4.157×10^{-2}	1
9.991×10^{-1}	9.588×10^{-1}	2.313×10^{-3}	3.145×10^{-2}	1
9.995×10^{-1}	9.681×10^{-1}	1.451×10^{-3}	2.397×10^{-2}	1
9.999×10^{-1}	9.908×10^{-1}	1.160×10^{-4}	6.701×10^{-3}	1
1	1	6.300×10^{-5}	5.332×10^{-3}	1
• 1.2×10^{33}	4×10^{10}	82.586	8.557×10^{6}	1.1905×10^{33}

• Scaling factors.

CHAPTER V

CONCLUSION

Evolutionary sequences of Stellar Models are constructed for the low mass stars in the mass range 0.30 $M_\odot$ – 0.60 $M_\odot$ using the recent values and method of evaluation for some of the input physics.

It is established that the 0.30 $M_\odot$ star develops a small radiative core but reaches the ZAMS as wholly convective star in 6.95×10^8 years. The behaviour of the internal structure of the 0.40 $M_\odot$, 0.50 $M_\odot$ and 0.60 $M_\odot$ stars is similar to each other during the evolution, except that the 0.40 $M_\odot$ star has the largest convective core when it is on the main – sequence position.

Comparing our theoretical models with the observation led us to the conclusion that HR 6426 B is a star near the ZAMS having an age of about 1.08×10^8 years with the central temperature and density of 9×10^6 K^0 and 78 gr/cc, respectively.

The isochrones obtained from the present study give an age of about 6×10^6 years for the T Tauri stars belonging to the Taurus Auriga Molecular Cloud Complex which is in good agreement with the one given by Herbig[33].

Some important remarks must be made on the conclusions.
The conclusions we arrived as a result of the present study certainly are affected by the same sources of errors both in observational and theoretical calculations. From the point of view of the theoretical calculations different results , and may be better fit to the observations, can be obtained by choosing a real opacity corresponding to a real composition of the star under consideration. Even a moderate change in the value of $\alpha = l/H_p$ in the convective theory will have significant

effect on the overall structure of the stars since nearly all the physical parameters are sensitive to the value of the mixing–length parameters used. In comparing the results of the present study with that of previous works, small differences can be seen. These are partly due to the different methods used in the construction of models, the formulation of the EOS and variations in the thermonuclear reaction rates.

REFERENCES

[1] C. Hayashi and T. Nakano, Prog. Theoret. Phys. 30, 460 (1963).

[2] D. Eryurt - Ezer and A. G. W. Cameron Can. J. of Phys. 45 , 3461 (1963).

[3] H. Copeland, J. O. Jensen and H. E. Jorgensen, Astr. Ap. 5, 12 (1970).

[4] D. T. Hoxie, Astr. Ap., 26, 437 (1973).

[5] A. S. Grossman, D. Hays and H. C. Graboske, Astr. Ap., 30 , 95 (1974).

[6] R. Sienkiewicz, Acta Astronomica, 32, 275 (1982).

[7] D. A. VandenBerg, F. D. A. Hartwick, P. Dawson and D. R. Alexander, Ap. J., 266, 747 (1983).

[8] S. Rappaport and P. C. Joss, Ap. J., 283, 232 (1984).

[9] G. D. Neece, Ap. J., 277, 738 (1984).

[10] F. D'Antona and I. Mazzitelli, Ap. J., 296, 502 (1985).

[11] L. A. Nelson, S. A. Rappaport and P. J. Joss, Ap. J., 311, 226 (1986).

[12] B. Dorman, L. A. Nelson and W. Y. Chau,Ap. J. 342, 1003 (1989).

[13] P. P. Eggleton, J. Faulkner and B. P. Flannery, Astr. Ap. 23, 325 (1973).

[14] A. N. Cox and J. E. Tabor, Ap. J. Suppl., 31, 271 (1976).

[15] G. Magni and I. Mazzitelli, Astr. Ap., 72, 134 (1979).

[16] D. R. Alexander, H. R. Johnson and R. L. Rympma, Ap. J., 272, 773 (1983).

[17] D. R. Alexander private communication, (1986)

[18] W. A. Fowler, G. R. Caughlan and B. A. Zimmerman, Ann. Rev. Astr. Ap., 13, 69 (1975).

[19] M. J. Harris, W. A. Fowler, G. R. Caughlan and B. A. Zimmerman, Ann. Rev. Astr. Ap., 21, 165 (1983).

[20] C. A. Rouse, Ap. J., 139, 339 (1964).

[21] N. Itoh, H. Totsuji, S. Ichimaru and H. E. DeWitt, Ap. J., 234, 1079 (1979)

[22] E. Böhm - Vitense, Zeit. Ap., 46, 108 (1958).

[23] J. P. Cox, and R. T. Guili, Principles of Stellar Structure, I, II, (1968).

[24] L. Motz, Astrophysics and Stellar Structure, Massachusetts (1970).

[25] D. Eryurt-Ezer, Write - Up for the computer program, Special print (1972).

[26] E. E. Salpeter ,Ap. J., 134, 669 (1961)

[27] E. E. Salpeter and H. M. Van Horn,Ap. J., 155, 183 (1969)

[28] A. Alastuey and B. Jancovici,Ap. J., 226, 1304 (1978)

[29] D. Eryurt - Ezer and A. G. W. Cameron, Ap. and Sp. Sc. 10, 52 (1971).

[30] C. A. Iglesias, F. J. Rogers and B. G. Wilson Ap. J., 397, 717 (1992)

[31] R. Stother and C. Chin, Preprint. (1993).

[32] D. Popper, Ann. Rev. Astron. Astrophys. 18, 115 (1980).

[33] S. W. Stahler, Ap. J. 332, 804 (1988).

[34] G. H. Herbig, Ap. J. 217, 693 (1977).

CURRICULUM VITAE

The author of this work was born in 1960 in İstanbul as a Turkish citizen.
He received his B.Sc. degree in 1985 and his M.Sc. degree in 1987 in Physics from Department of Physics of Middle East Technical University (METU).
Since 1986 he has been worked as a research assistant in METU,
Physics Department.
He has two paper related with "Ages of Clusters" and "Observations of $\delta-$ Scuti type Pulsators"(joint paper).
He is married and has a boy and a daughter.